

**PHOSPHATE ANALOGUES AS PROBES OF THE CATALYTIC
MECHANISMS OF MURA AND AROA, TWO CARBOXYLVINYL
TRANSFERASES**

**PHOSPHATE ANALOGUES AS PROBES OF THE CATALYTIC
MECHANISMS OF MURA AND AROA, TWO CARBOXYLVINYL
TRANSFERASES**

By

FUZHONG ZHANG B.Sc.

A thesis submitted to the faculty of graduate studies in the partial
fulfillment of the requirements for the degree of Master of Sciences

McMaster University

© Copyright by Fuzhong Zhang, August 2005

Title: Phosphate Analogues as Probes of the Catalytic Mechanisms of MurA and AroA, Two Carboxyvinyl Transferases

Author: Fuzhong Zhang B.Sc. (Peking University, Beijing, P.R.China)

Supervisor: Dr. Paul J. Berti

Number of Pages: 95

Abstract

The two carboxyvinyl transferases MurA and AroA are essential for bacterial survival, and are proven or potential antibiotic targets. The reactions they catalyze are chemically challenging, involving protonation of an ethylene group in the first step, and deprotonation of a methyl in the second step. In order to probe how the enzymes promote these reactions, the reverse reactions from enolpyruvyl compounds (EP-OR) plus phosphate to phosphoenolpyruvate (PEP) plus R-OH were investigated, and compared with EP-OR hydrolysis reactions catalyzed by phosphate analogues.

Thirteen phosphate analogues were used to study EP-OR hydrolysis. Among these phosphate analogues, many could bind to the free enzymes, but only three could promote hydrolysis. The products were pyruvate and the corresponding alcohol (S3P in AroA/EPSP reaction and UDP-GlcNAc in MurA/EP-UDP-GlcNAc reaction). The most effective analogue was arsenate. The mechanism of the arsenate-promoted reaction was examined in detail. The hydrolysis reaction proceeded through an arseno-tetrahedral intermediate with AroA, a similar reaction pathway to the natural reaction. This arseno-tetrahedral intermediate was converted to arsenoenolpyruvate and hydrolyzed spontaneously. MurA also likely catalyzed arseno-tetrahedral intermediate formation, and

appeared to catalyze arsenoenolpyruvate breakdown, though it is possible that it was a bystander in the reaction, with the tetrahedral intermediate being formed by water attack on C2 of EP-UDP-GlcNAc. There was a fast solvent exchange step before EP OR was converted to arseno-THI by AroA or MurA. This strongly indicated an oxacarbenium ion like intermediate before the arseno-tetrahedral intermediate.

The catalytic machinery for stabilizing such an unstable oxacarbenium ion like intermediate was investigated by studying ligand binding. Based on information from all the phosphate analogues, there were evidence that the enzyme undergoes a conformational change upon binding with phosphate, by which EPSP was distorted into an oxacarbenium ion like intermediate.

Acknowledgement

First, I would like to thank Dr. Paul Berti for giving me the opportunity to come to McMaster University and introducing me to the amazing scientific world. This work, plus the continuing work on KIE measurement in EP-UDP-GlcNAc hydrolysis reactions were under assistance from McMaster University mass spectrometry facility. As well, I thank Dr. Paul Loncke for his great help in the computational section, Joe McCann for his constant ideas and support. I thank Meghann Clark and other lab members in creating such a fantastic environment. Thank you to all my family members for their encouragement and support. Finally, I would like to thank my beloved girl friend, Jinyu Du, for all the hard time she got through together with me, even far away from China. I could not have done this without her unending encouragement.

Table of Contents

Abstract.....	iii
Acknowledgement.....	v
Abbreviations	x
1 Introduction	1
1.1 MurA and AroA, two carboxyvinyl transferases	1
1.2 Good targets for developing antimicrobials.....	2
1.3 General acid base catalysis and tetrahedral intermediate	3
1.4 Evidence of oxacarbenium ion in addition steps	4
1.5 Mechanism in elimination steps.....	7
1.6 Important catalytic residues	8
1.7 Mechanism based inhibitor and transition state analogue	12
1.8 Reverse Reaction	13
1.9 Reaction coordinate in MurA-catalyzed reaction.....	18
1.10 Non-enzymatic THI breakdown.....	18
1.11 Phosphate analogues	20
2 Experimental	24
2.1 General.....	24
2.2 Enzyme purification and compounds synthesis	25
2.2.1 <i>E. coli</i> MurA expression and purification.....	25
2.2.2 <i>E. coli</i> AroA _{H6} expression and purification	27

2.2.3	<i>E. coli</i> PPDK expression and purification	27
2.2.4	[1- ¹⁴ C]PEP and [¹³ C]PEP synthesis.....	28
2.2.5	EP-UDP-GlcNAc and EPSP synthesis	29
2.2.6	[1- ¹⁴ C]THI (MurA) synthesis	30
2.3	MurA THI enzymatic breakdown.....	30
2.4	Phosphate analogue/enzyme-catalyzed EP-OR hydrolysis products	32
2.4.1	Products characterization by HPLC.....	32
2.4.2	Products characterization by Radioactivity assay.....	32
2.4.3	Lactate Dehydrogenase reaction assay	33
2.4.4	Products characterization by Mass spectrometry	33
2.5	Kinetics of phosphate analogues/enzyme-catalyzed EP-OR hydrolysis.....	33
2.6	Mechanism of arsenate/enzyme-catalyzed EP-OR hydrolysis.....	34
2.6.1	Phosphate analogue/enzyme-catalyzed EP-OR C3 proton solvent exchange	34
2.6.2	[3- ³ H]EP-OR hydrolysis	36
2.6.3	EP-OR hydrolysis in H ₂ ¹⁸ O.....	37
2.7	Fluorescence titration experiments	37
2.8	Phosphate analogues charge calculation	39
3	Result.....	40
3.1	Enzyme purity, concentration and specific activity measurement.....	40
3.2	Ligands synthesis	41

3.3	MurA THI enzymatic breakdown	44
3.4	Phosphate analogue/enzyme-catalyzed EP-OR hydrolysis products	45
3.4.1	Products characterization by HPLC.....	45
3.4.2	Products characterization by radioactivity assay	48
3.4.3	Lactate Dehydrogenase reaction assay	50
3.4.4	Products characterization by mass spectrometry	51
3.5	Kinetics of phosphate analogue/enzyme-catalyzed EP-OR hydrolysis.....	51
3.6	Isotope labeling experiments	53
3.6.1	Phosphate analogue/enzyme-catalyzed EP-OR C3 proton solvent exchange	54
3.6.2	[3- ³ H]EP-OR hydrolysis	57
3.6.3	EP-OR hydrolysis in H ₂ ¹⁸ O	59
3.7	Fluorescence titration experiments	61
3.7.1	Free enzyme titration.....	62
3.7.2	EPSP titration to enzyme analogue complex.....	65
3.7.3	Second step titration with D313A.....	68
3.8	Phosphate analogue charge calculation	69
4	Discussion.....	71
4.1	MurA THI enzymatic breakdown	71
4.2	Mechanism of arsenate-promoted EP-OR breakdown.....	72
4.3	Oxocarbenium ions	79

4.4 Phosphate analogue binding pocket.....	82
4.5 Two conformational changes upon substrate binding.....	83
4.6 Phosphate analogues	84
5. Conclusions.....	88
6. References.....	90

Abbreviations

AroA	5- <i>enol</i> pyruvyl shikimate 3-phosphate synthase
AroA _{H6}	AroA containing a C-terminal His ₆ sequence
DTT	dithiothreitol
EP-OR	either EPSP or EP-UDP-GlcNAc
EPSP	5- <i>enol</i> pyruvyl shikimate 3-phosphate
EP-UDP-GlcNAc	<i>enol</i> pyruvyl uridine diphosphate <i>N</i> -acetyl-glucosamine
$K_{d,L}$	equilibrium dissociation constant of enzyme with ligand
L	
LDH	lactate dehydrogenase.
MurA	UDP-GlcNAc <i>enol</i> pyruvyl transferase
NADH	nicotinamide adenine dinucleotide;
NPA	Natural Population Analysis
PEP	phospho <i>enol</i> pyruvate
S3P	shikimate 3-phosphate
THI	tetrahedral intermediate
TS	transition state
UDP-GlcNAc	uridine diphosphate <i>N</i> -acetylglucosamine

Introduction

1.1 MurA and AroA, two carboxyvinyl transferases

MurA (UDP-GlcNAc enolpyruvyl transferase) and AroA (EPSP synthase) are the only two enzymes found to date to catalyze carboxyvinyl transfer. MurA catalyses the first committed step in peptidoglycan biosynthesis (1), which is the main component of the bacterial cell wall. It transfers the carboxyvinyl group of phospho*enol*pyruvate (PEP) to the 3'-hydroxyl of UDP-GlcNAc, yielding EP-UDP-GlcNAc (Fig. 1) (2, 3). AroA is in the shikimate pathway leading to aromatic compounds in microorganisms and plants (4). It transfers the same carboxyvinyl group of PEP to shikimate-3-phosphate, yielding EPSP (5, 6). Both reactions are reversible.

MurA and AroA are homologous, sharing the same overall three-dimensional architecture: two globular inside-out α/β -barrel domains connected by a two-stranded hinge (7). Both undergo substrate-induced conformational changes that form the active center for catalysis, and which can be monitored by fluorescence changes (5, 8).

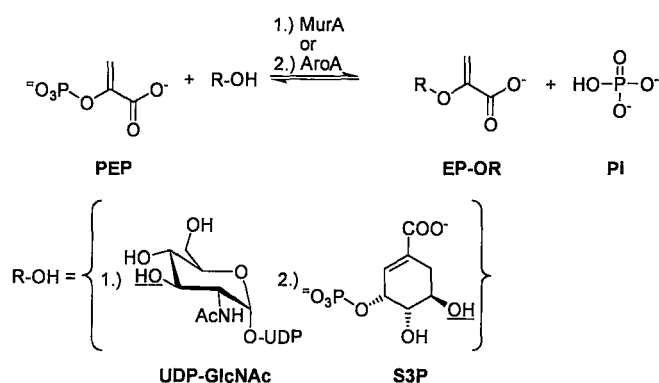


Figure 1. Reactions catalyzed by MurA and AroA.

1.2 Good targets for developing antimicrobials

The reaction catalyzed by MurA is in the pathway leading to peptidoglycan in bacteria. Peptidoglycan is a crosslinked carbohydrate polymer that comprises bacterial cell walls, enabling the cells to withstand extreme osmotic pressure fluctuations. Damage to the peptidoglycan layers results in bacterial cell death (9). Because peptidoglycan biosynthesis is highly conserved in eubacteria (9), it is a prime target for broad spectrum antibiotics. EP-UDP-GlcNAc is a precursor in the peptidoglycan biosynthesis pathway. MurA catalyzes the formation of EP-UDP-GlcNAc from UDP-GlcNAc. Inhibition of this enzyme provides an efficient way to kill bacteria.

The aromatic amino acids tyrosine, phenylalanine and tryptophan are synthesized by bacteria (including pathogenic bacteria), parasites, and plants. But these biosynthetic pathways are missing in vertebrates. The

aromatic amino acids can be only obtained from degradation of dietary proteins. The lack of aromatic biosynthetic pathways provides good targets for developing antimicrobials. AroA, one enzyme in the pathway, catalyzes the formation of EPSP.

There are inhibitors for both carboxyvinyl transferases. Fosfomycin, a broad-spectrum antibiotic, inhibits of MurA with IC_{50} approximately 1 μ M (10). It alkylates Cys115, a general acid residue in *E. coli* MurA. However Cys115 is not conserved in all bacteria, being Asp in MurA from tuberculosis and other pathogenic organisms, which are fosfomycin resistant (11). AroA is inhibited by glyphosate, a herbicide which inhibits both AroA and its orthologue in plants (12, 13), but it is not an antibiotic.

Bacterial survival strongly depends on the functionality of a unique class of enzymes, carboxyvinyl transferases. They are good targets for developing antimicrobials.

1.3 General acid base catalysis and tetrahedral intermediate

The reaction mechanisms of both MurA and AroA have been studied intensively with pre-steady state experiments (11, 14, 15), site-directed mutagenesis (11), substrate analogues (16-18), x-ray crystallography (7, 19, 20), fluorescence titration (21) and NMR experiments (6, 22). Their mechanisms are similar in several aspects.

Both are believed to use general acid-base catalysis (23). The reactions are easily reversible, proceeding via an addition-elimination pathway through a non-covalently bound tetrahedral intermediate (THI) (14, 15) (Fig. 2).

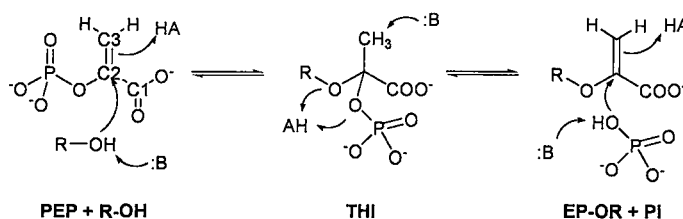


Figure 2. MurA/AroA reaction pathways, proceeding through a tetrahedral intermediate (THI).

In the addition step, the ethylene group of PEP is protonated at C3 by the general acid and C2 was attacked by the hydroxyl oxygen from the corresponding alcohol (UDP-GlcNAc in the MurA reaction and S3P in the AroA reaction) with the help of general base. A tetrahedral intermediate can be isolated by denaturing the enzyme under basic conditions. In the elimination step, the C3 methyl is deprotonated by a general base catalyst and inorganic phosphate is eliminated.

1.4 Evidence of oxacarbenium ion in addition steps

Even though the mechanism has been widely studied for several decades, there are still several mechanistic controversies. The mechanism for the addition step from PEP, and alcohol to THI is relatively clear. There

were several pieces of evidence suggesting an oxacarbenium ion transition state.

In MurA, Brown et al. first characterized a phospholactoyl-enzyme adduct (24), where PEP was covalently linked to the enzyme at Cys115. This was later studied in more detail with fluoro-labeled PEP (16). It was found that the formation of phospholactoyl-enzyme adduct was slower than fluoro-THI, and it only occurred when UDP-GlcNAc was in present (Fig. 3). They concluded that PEP inside the catalytic center was protonated and the enzyme stabilized an oxacarbenium ion upon binding with UDP-GlcNAc. The substrate-induced conformational change was later demonstrated in both crystal structure (7, 25, 26) and fluorescence experiments (21).

The oxacarbenium ion was also supported by site-directed mutagenesis experiments (11). When Cys115 was mutated to Asp, the enzyme lost the ability to be inhibited by fosfomycin. The inhibitor of MurA, fosfomycin, can be irreversibly attached to Cys115 and form a covalently fosfomycin adduct, thus alkylating the proposed catalytic base and taking the position of PEP in the active centre of MurA. The loss of inhibition by fosfomycin in C115D is consistent with this mechanism. However, C115D is still active. Its k_{cat} is even higher than wild-type MurA at pH from 5.5 to 7. This suggested that the phospholactoyl-enzyme adduct is not necessary

for catalysis. It is also consistent with Asp, a better oxocarbenium ion stabilizer, lowering the energy of TS further.

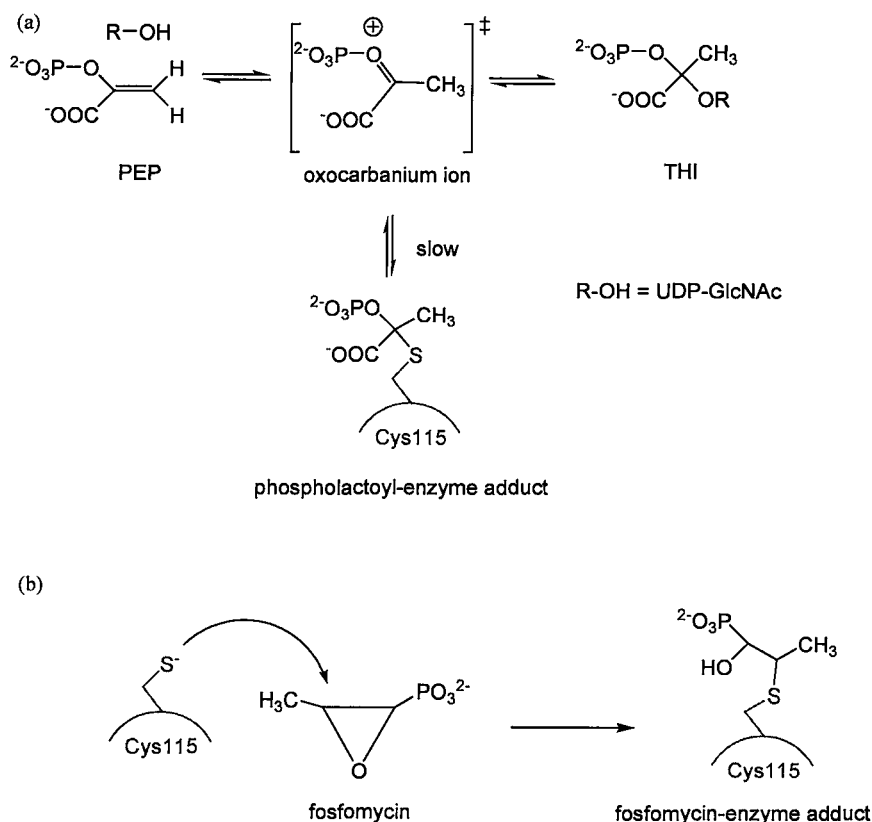


Figure 3. Oxocarbenium ion-like TS during the addition step of MurA reaction. (a) The phospholactoyl-enzyme adduct was believed a side product of the reaction. (b) Fosfomycin inhibition mechanism.

Evidence for an oxocarbenium ion during the addition step in the AroA reaction is more straightforward. Upon incubating AroA with dideoxyS3P (ddS3P), where the nucleophilic hydroxyl was missing, Anton et al. observed tritium was incorporated from water into the C3 of PEP without formation of any EPSP or THI (27). This strongly suggested that C3 was protonated inside the active site and formed the

oxocarbenium ion form of PEP. This oxocarbenium ion exists long enough for the C3 to rotate, and one of the methyl protons to be removed during deprotonation, allowing tritium to remain in PEP. The formation of the oxocarbenium ion also requires a conformational change in AroA, which was monitored by fluorescence titrations (21).

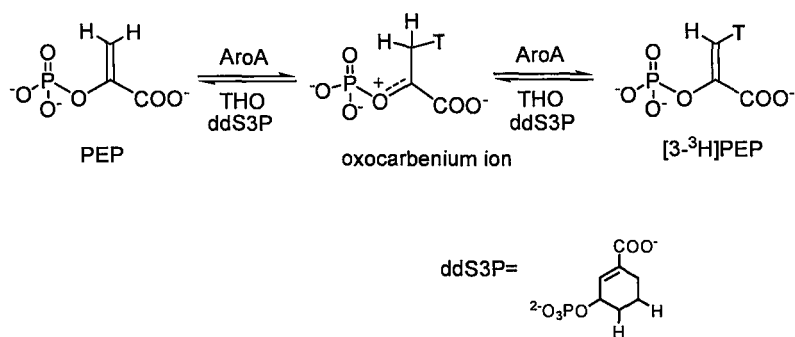


Figure 4. Oxocarbenium ion form in the addition step of AroA-catalyzed reaction, showing that tritium can be incorporated into C3 of PEP.

1.5 Mechanism in elimination steps

The detailed mechanism of the elimination step is not clear. Based on the lack of formation of a fluoro-EP-UDP-GlcNAc like product from fluorine substituted THI, Walsh and coworkers believed it went through an oxocarbenium ion intermediate (11). They assumed an E2-type mechanism for the elimination step would not be affected by the substitution of fluorine at C3. In contrast, An et al. assigned the stereochemical course of AroA reaction and found the second step in AroA reaction went through a syn elimination (28). They referred to the

position of previous proposed catalytic base Glu341, which was orientated 90° to the other leaving group, phosphate, based on crystal structures (Fig. 6). For a syn elimination, this angle would be expected to be 180° . They pointed out the inconsistency and proposed a phosphate-assisted concerted mechanism, where phosphate acts as a base (Fig. 5).

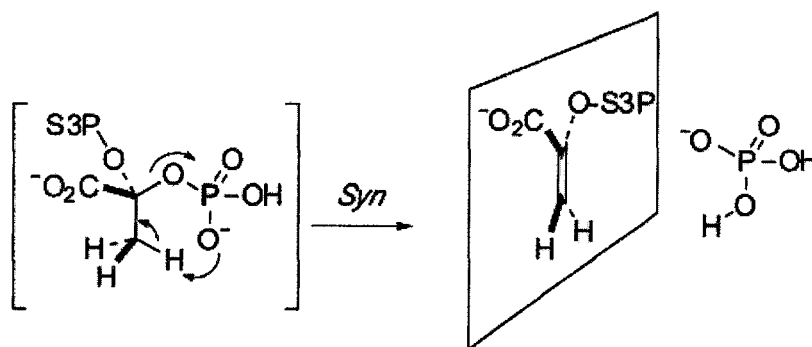


Figure 5. Proposed AroA-catalyzed elimination step. The syn elimination is consistent with phosphate assisted deprotonation.

1.6 Important catalytic residues

Even though people agree the overall reaction is general acid-base catalyzed. The catalytic residues are still disputed.

In MurA, Cys115 is the most interesting residue. It can be alkylated by fosfomycin, inhibiting the enzyme. PEP also interacts with it to form a covalently linked phospholactoyl-enzyme adduct. Cys115 is located in a loop which undergoes a large conformational change as the enzyme binds to the substrates (26). Site-directed mutagenesis experiments suggest it

acts as a general acid in protonating the C3 position in the addition step, and a general base for decomposition of THI in both forward and backward directions (11). Its pK_a inside the enzyme was determined to be 8.3, suggesting that Cys115 is appreciably protonated at physiological pH (29). This supported Cys115 as a general acid.

In AroA, Glu341, the equivalent residue to Cys115 in MurA, was proposed to act dual role in both protonation of C3 of PEP and deprotonation of THI (30).

However, results from combination of stereochemistry and crystal structure indicated Cys115 and Glu341 are not well aligned with phosphate for a syn elimination in the second step (Fig. 6). Both Duncan (19) and Bartlett (28) pointed out that phosphate could act as an intramolecular proton acceptor.

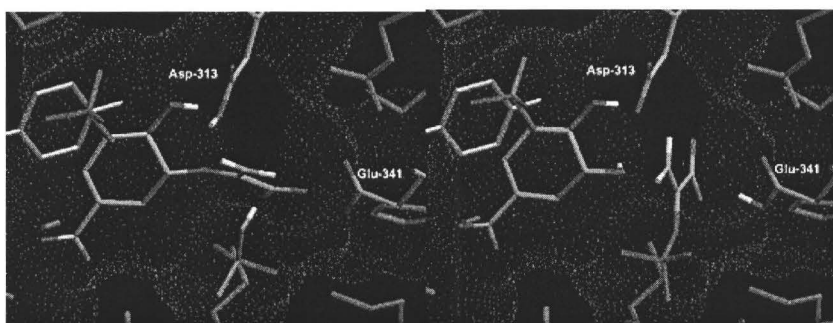


Figure 6. Residues in AroA catalytic centre from X-ray crystallography. Glu341 was orientated 90° to the phosphate moiety based on this crystal structure, which is not consistent with the expected 180° for syn elimination.

The catalytic base which deprotonates the alcohol is

another unresolved problem. Asp305 was demonstrated to be important for the catalysis in MurA. Samland et al. showed D305A, D305C, D305H mutant proteins did not have detectable enzymatic activity (25, 31). They argued that Asp305 serves as both a general base and an essential binding partner to UDP-GlcNAc in the addition step. Its equivalent residue Asp313 in AroA was proposed to have the same role by Schonbrunn and co-workers from crystal structure (25). However, this was not consistent with former proposed base Lys22 in AroA, which also located close to S3P C5 oxygen (32). The pK_a of this residue was measure to be 7.6, lower than a normal Lys side chain (approximately 10.8), ensuring enough deprotonated form at physiological condition.

More recently, Mizyed et al. from this lab studied the effects of active site mutations on the partitioning of THI (30). While many mutations reduced the catalytic activity significantly, none produced a large change in the partition ratio. This indicated “ensemble catalysis” with a large number of residues being important for catalysis. Among them, Glu341 and Lys22 act as the dual-role acid/base catalysts; that is Glu341 would be the proton donor in formation of the THI from S3P and PEP and the proton acceptor in elimination of the THI to EPSP and phosphate. Lys22 would serve as the proton acceptor from S3P in the addition step and proton donor for phosphate elimination.

Making it more complicated, a new view of the two carboxyvinyl transferases from x-ray structures of their THI states was published by Schonbrunn and co-workers (33). They made D305A mutation for MurA and D313A for AroA. Their experiments showed the reaction stopped after formation of THI. They measured distance between Cys115 (MurA)/Glu341 (AroA) and C3 carbon of THI from the crystal structures of the two mutations. They were 7.0Å and 3.4Å respectively. They concluded that these residues were too far away to deprotonate C3 methyl. However, they noticed the carboxylate groups of the modeled Asp side chains are in good hydrogen-bonding distance to the 4'-OH of the UDP-GlcNAc (2.7 Å) in MurA, and to the 4-OH of the S3P in AroA. These hydroxyls are close to the hydroxyls where the bonds are forming during the reaction, 3.4 Å and 3.1 Å in MurA and AroA respectively. They proposed that the deprotonation of C3 THI methyl group might proceed intramolecularly, where Asp residues abstracts the proton from 4-OH (or 4'-OH in MurA), the resulting oxyanion then would abstract a proton from C3 methyl (Fig. 7).

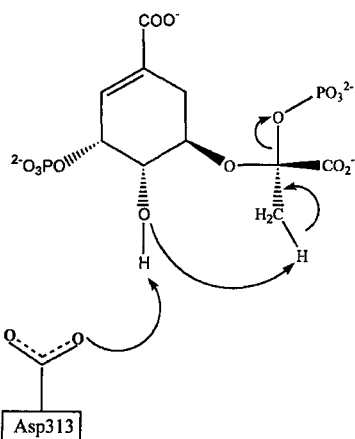


Figure 7. Proposed mechanism in AroA-catalyzed reaction, where D313 serves as catalytic base.

Overall, there are many disputed aspects on the mechanism of the two carboxyvinyl transfer reactions. Studying the mechanism of the two enzymes is still necessary.

1.7 Mechanism based inhibitor and transition state analogue

Enzymes catalyze reactions by lowering the energy of the transition state(s) (TS). In any reaction, the transition state (TS) is the highest energy point in the energy profile. Enzymes exert their catalytic activity by binding tightly with TS rather than substrates or products (34), stabilizing the TS, and lowering the activation energy of the reaction (Fig. 8). As compared with equilibrium dissociation constants with substrates or products, which are generally in the 10^{-3} to 10^{-6} M range, equilibrium dissociation constant can be as low as 10^{-13} M for the enzyme•TS complex. An effective way to inhibit an enzyme is to mimic the TS. Such

an inhibitor is called a transition state inhibitor, which would be extremely difficult for the enzyme to evolve other catalytic machinery to avoid.

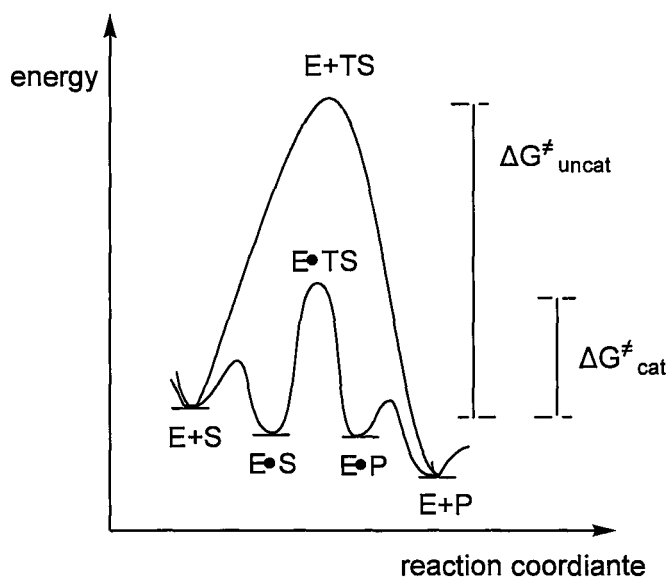


Figure 8. Enzymatic transition state stabilization. Black line, reaction pathway without enzyme. Red line, pathway of enzyme-catalyzed reaction. Enzymes catalyze reactions by binding with transition state, lowering the activation energy.

Determination of TS structures can help us to understand enzyme mechanisms, and, what is more important from the application point of view, design of TS analogues. TS analogues are stable molecules having almost the same structure as TS, which can bind with enzymes almost as tightly as TSs. TS analogues would be potential lead compounds for novel effective inhibitors. All of these will provide us a clear clue for drug design. So there is significant need to study the structure of TSs.

1.8 Reverse Reaction

In the reverse reaction of the two carboxyvinyl transferases, phosphate reacts with EP-OR, yielding THI in the first step. THI is then converted into PEP and the corresponding alcohol. In the first step, phosphate is covalently linked to C2 carbon to form a C-O bond. The challenge is to understand how the enzyme takes phosphate, a small, poor nucleophile, to undertake a nucleophilic attack at C2 carbon, a non-reactive site. The exact mechanism of this step was not known; it could be either a stepwise mechanism, with protonation of C3 occurring to form a cationic intermediate before nucleophilic attack at C2, or an asynchronous concerted addition step with significant cationic character at C2.

Phosphate is a biologically important molecule. It is involved in countless processes such as biosynthetic pathways, protein post-translational modifications and regulation of signal transduction. At an oxidation state of +5, the phosphorus atom (including those in phosphate esters) does not react readily as a nucleophile, but as electrophile, undergoing attack by a variety of other nucleophiles. For example, phosphatases and phosphodiesterases take water as a nucleophile to attack phosphorus; kinases use other nucleophiles to transfer a phosphoryl group PO_3 , where phosphorus is still an electrophile.

However, there are rare cases that phosphate is used as a nucleophile. In phosphorylases, inorganic phosphate, specifically one of

the anionic oxygen atoms, serves as a nucleophile. Saccharide phosphorylases transfer the glucosyl group to phosphate and form sugar-1-phosphate in most of cases. The reaction has either S_N1 or S_N2 mechanisms. In the cellobiose phosphorylase (35) and maltose phosphorylase (36), the disaccharide was cleaved at the oxygen-bridge bond, yielding glucose-1-phosphate and another free glucose. The configuration of C1 is inverted from substrate to product in both of the two enzymatic reactions. This implied a direct S_N2 displacement by the inorganic phosphate at C1 of the disaccharide moiety. (Fig. 9)

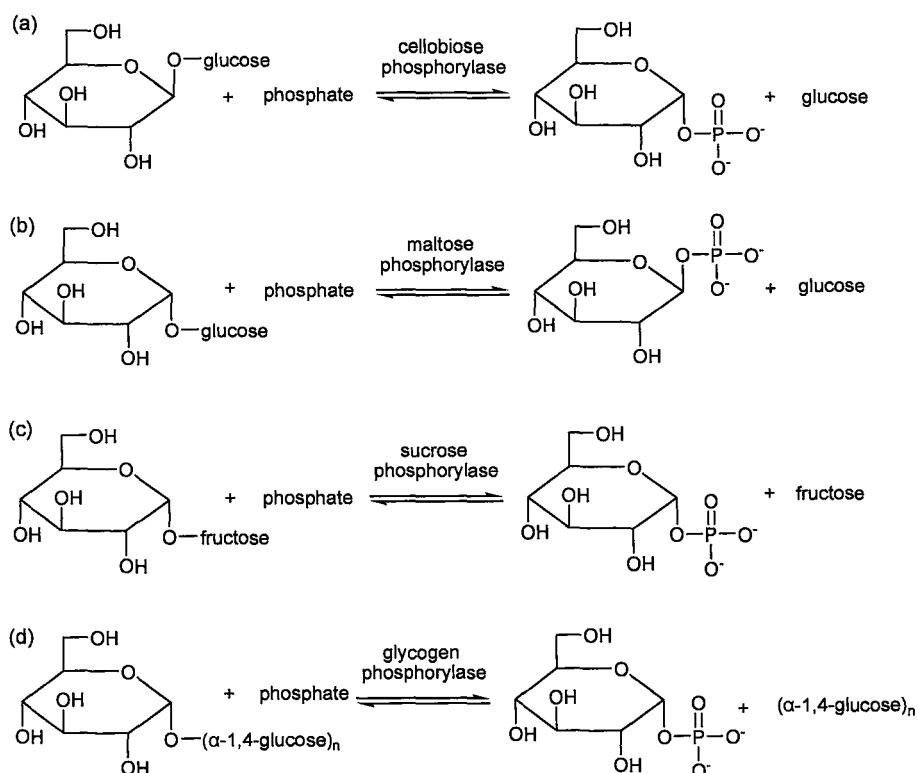


Figure 9. Reactions catalyzed by phosphorylases where phosphate is used as a nucleophile. Reaction catalyzed by (a) cellobiose phosphorylase and (b) maltose phosphorylase have conformation inversion at C1, indicating S_N2 mechanism. Reaction

catalyzed by (c) sucrose phosphorylase and (d) glycogen phosphorylase proceed with retention of conformation.

If the configuration at C1 is retained, the mechanism could be either two S_N2 displacements (double inversion) or S_N1 with exclusive front side attack due to the shielding by the enzyme. In sucrose phosphorylase (37-39), ^{14}C in fructose (the free sugar product) is incorporated into the sucrose in the absence of inorganic phosphate. This suggests an enzyme covalently linked adduct is involved in the reaction (Fig. 9c, Fig. 10a), where the enzyme attacks C1 and releases fructose. The ^{14}C labeled fructose was incorporated into sucrose by the reverse reaction of this step. In another experiment, arsenolysis of glucose-1-phosphate by this enzyme indicated that glucose-1-phosphate undergoes a normal reverse reaction to glucosyl enzyme, which is then attacked by arsenate (phosphate analogue) to form unstable glucose-1-arsenate, which is quickly hydrolyzed to glucose and arsenate (Fig. 10b). The enzyme adduct was later isolated and identified. The kinetic mechanism was shown to be a ping-pong BiBi substrate binding. All these supported a double S_N2 displacements mechanism. In glycogen phosphorylase (40, 41), which phosphorylates polysaccharides, evidence favours a S_N1 mechanism (Fig. 10c). (1) Initial-velocity measurements reveal a random kinetic mechanism; (2) The C1 configuration of the glucose is retained in glucose-1-phosphate. (3) There was no incorporation of ^{32}P into glucose-1-

phosphate when glucose-1-phosphate was incubated together with [^{32}P]-phosphate. These observations are consistent with a shielded C1 oxocarbenium ion mechanism.

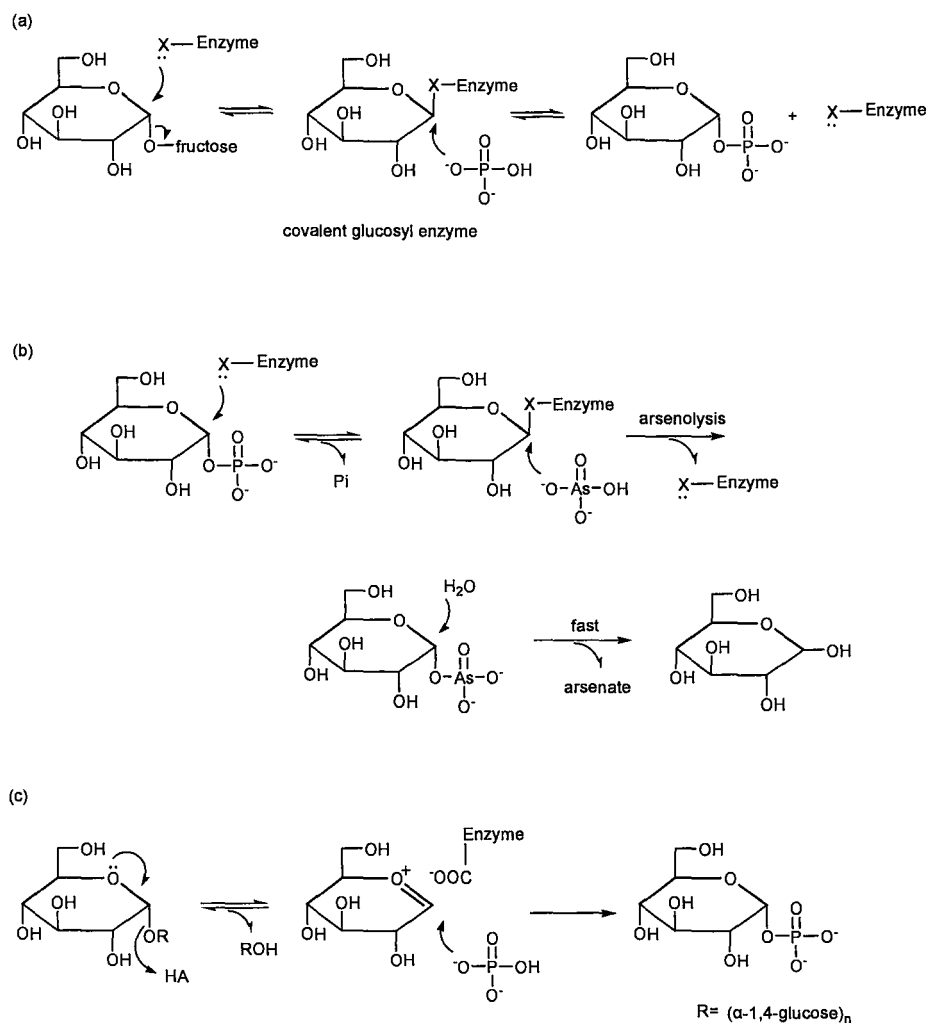


Figure 10. Phosphorylase Mechanisms. (a) sucrose phosphorylase. (b) arsenolysis catalyzed by sucrose phosphorylase. (c) glycogen phosphorylase.

In each enzyme, inorganic phosphate attacks a sp^3 hybridized carbon. There are rare cases that phosphate is taken as a nucleophile to

attack a sp^2 hybridized ethylene carbon as in AroA and MurA. So the question was if phosphate attack was concerted with C3 protonation, or a stepwise mechanism where C3 was protonated first. And how does the enzyme lower the energy barrier to make phosphate undergo a nucleophilic attack?

1.9 Reaction coordinate in MurA-catalyzed reaction

In the MurA-catalyzed reaction, a non-covalently linked THI is formed. This makes the reaction coordinate complicated, with at least two transition states and one intermediate, possibly more. The overall reaction is reversible, meaning that the THI can partition both forward and backward. Partitioning of the MurA THI was measured in this study for two reasons. One was that it was useful for interpreting the phosphate analogue results. As well, our ultimate goal is to perform transition state analysis on MurA. Kinetic isotope effects will reflect a mixture of steps, including partitioning of the THI, unless it partitions predominantly in one direction or the other. However, unlike AroA, which bound its THI and degraded it rapidly, MurA-catalyzed THI breakdown was very slow, and a new approach to measuring partitioning had to be developed.

1.10 Non-enzymatic THI breakdown

MurA THI is relatively stable as compared with most of other

enzyme THIs. It is acid-labile, with half-lives of about 1 s at pH 1, 1 h at pH 7.5, and 89 days at pH 12 at 25 °C (Fig. 11) (42). This allowed us to separate THI from the MurA reaction under basic conditions. The mechanism of non-enzymatic MurA THI breakdown was studied in detail by Bart Byczynski from this lab (42). The study showed that the rate and the product distribution are controlled by protonation of different functional groups. The products are predominately UDP-GlcNAc, pyruvate and inorganic phosphate under a large pH range, from 100% at pH<1.6 to 90% at pH>6.4 (Fig. 12). Protonation of the bridging oxygen of the phosphate moiety leads to THI breakdown through C-O bond cleavage with the formation of an oxacarbenium ion intermediate (or TS). Nevertheless, little is known about MurA-catalyzed THI breakdown.

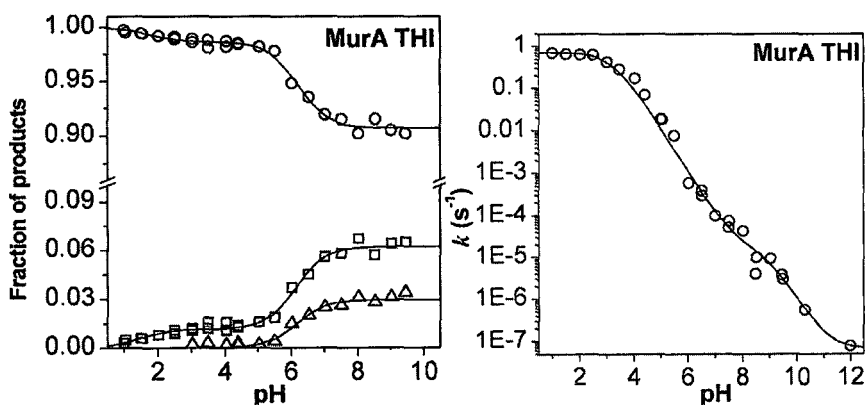


Figure 11. pH profile of MurA THI partitioning and breakdown (30).

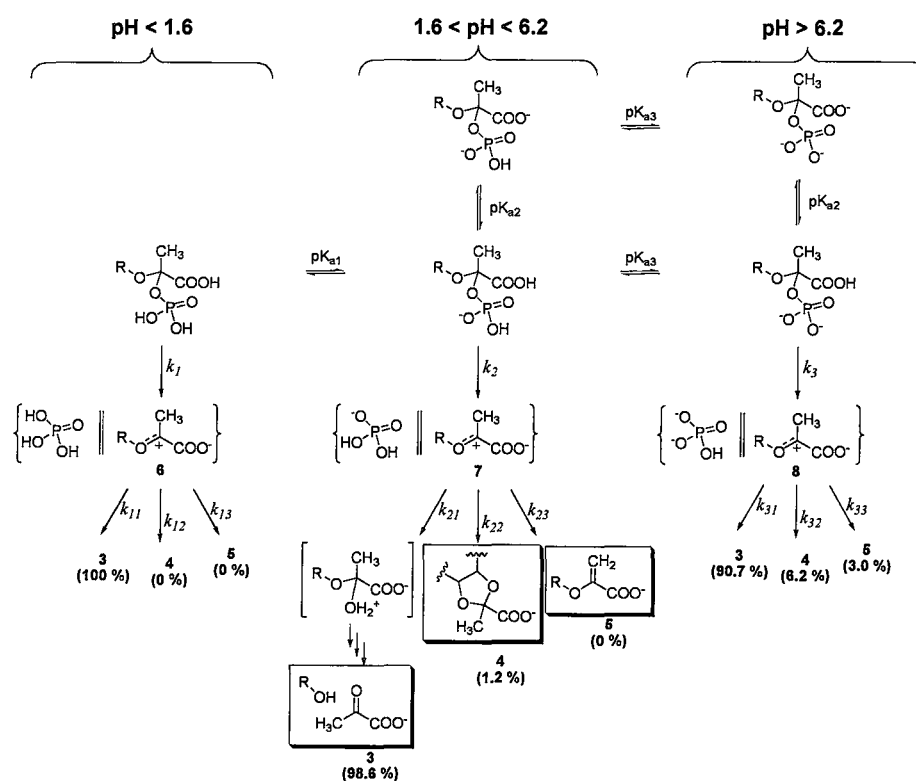


Figure 12. Mechanism of MurA THI non-enzymatic breakdown (42).

1.11 Phosphate analogues

Several molecules have been used as phosphate analogues in various studies. Among them, arsenate is probably the most common one. It is frequently accepted by enzymes, forming arsenate esters, which are quickly hydrolyzed to give inorganic arsenate and an alcohol (43). In glucose-6-phosphate isomerase (44), glucose and arsenate can reach a rapid equilibrium with glucose-6-arsenate, with equilibrium favouring dissociation (Fig. 13a). Glucose-6-arsenate is converted to fructose-6-arsenate and then hydrolyzed to fructose and arsenate. Glycerophosphate

dehydrogenase (45) reversibly catalyzes the oxidation of glycerol-3-phosphate to dihydroxyacetone phosphate (DHAP) using NAD^+ .

Incubation of dihydroxyacetone together with NADH in the presence of arsenate yields glycerol and NAD^+ (Fig. 13b). The mechanism was proposed to involve formation of dihydroxyacetone arsenate (a DHAP analogue) followed by conversion to glycerol-3-arsenate. This arsenate ester is later hydrolyzed by water non-enzymatically.

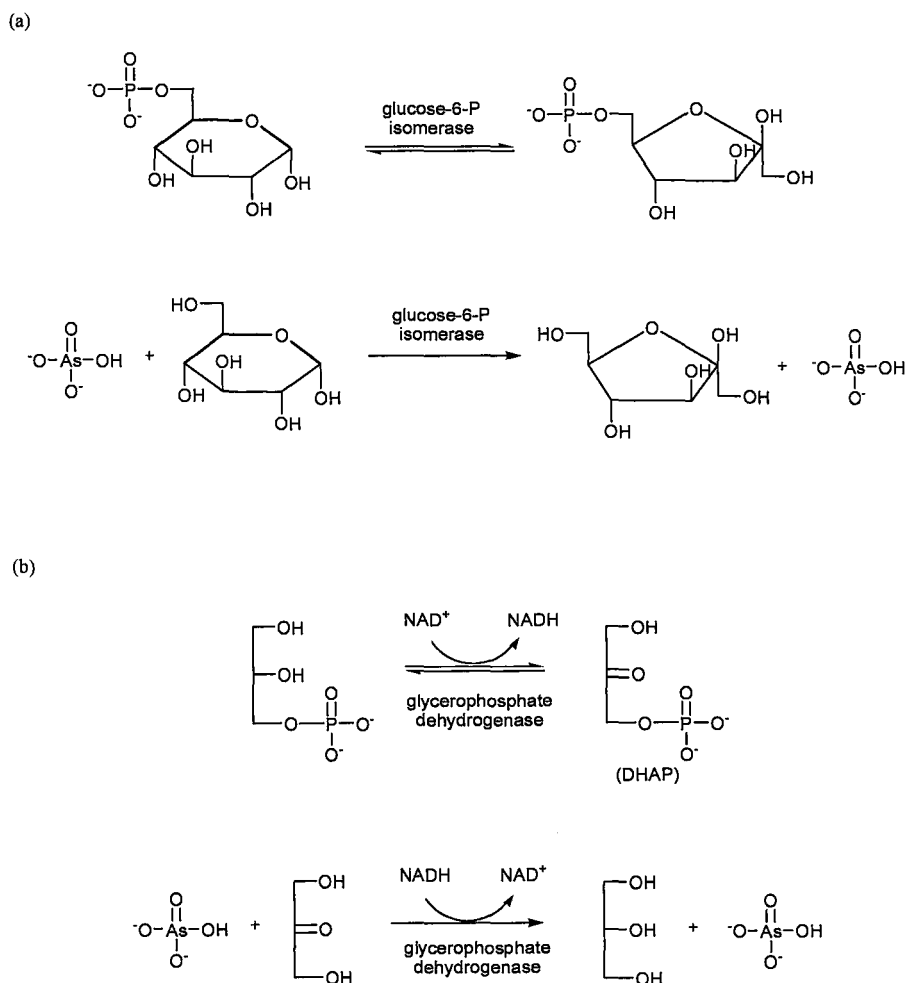


Figure 13. Arsenate as a phosphate analogue. (a) Reaction catalyzed by

glucose-6-P isomerase, and arsenolysis reaction. (b) Reaction catalyzed by glycerophosphate dehydrogenase and arsenate reaction.

In addition to arsenate, other phosphate analogues have been used. As with arsenate, substitution of phosphorus with element from transition metal vanadium yields another good analogue, vanadate. Vanadate inhibits many enzymes which catalyze phosphoryl transfer reactions, including mitochondrial ATPase (46). In glucose-6-phosphate dehydrogenase, it activates the oxidation of glucose by NADP^+ through formation of a transient glucose-6-vanadate (47) (Fig. 14). Tungstate, having the same tetrahedral geometry with phosphate was used to co-crystallize with protein-tyrosine phosphatase (48). Aluminum fluoride (AlF_x) is another commonly used phosphate analogue, especially in phosphoryl transferases as the transition state analog. A number of crystal structures of nucleotide binding proteins complexed with AlF_x have been determined in either AlF_4^- or AlF_3 (49) (50). Other, less commonly used phosphate analogues, including methyl phosphonic acid, methyl phosphate, thiophosphate and fluorophosphates, can also be useful in probing enzyme mechanisms.

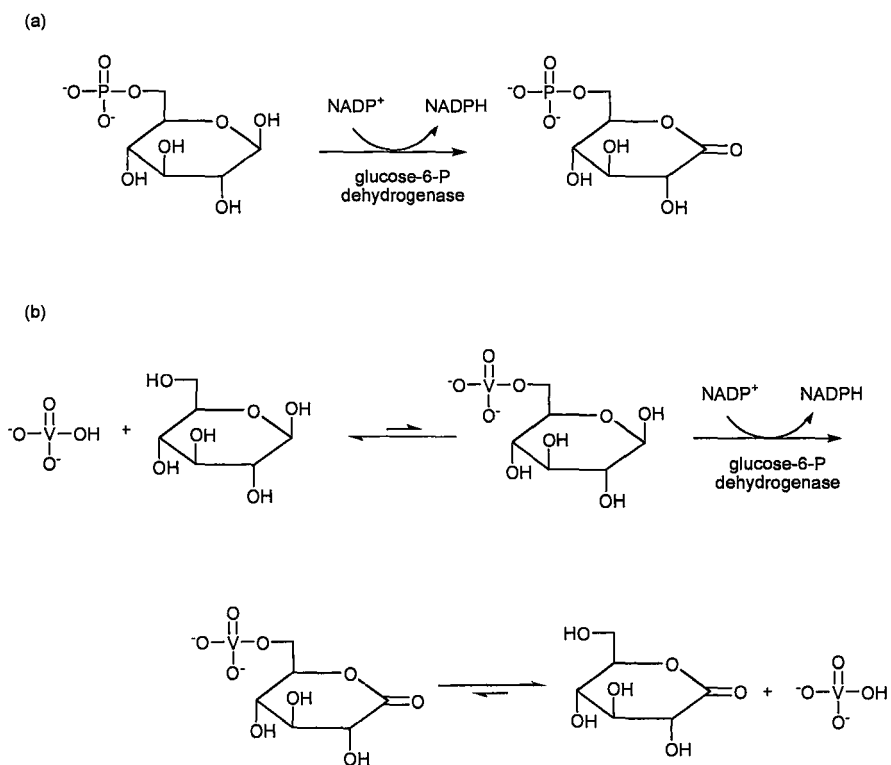


Figure 14. Vanadate as a phosphate analogue. (a) Reaction catalyzed by glucose-6-P dehydrogenase. (b) Vanadate assisted oxidation of glucose.

2 Experimental

2.1 General

UDP-GlcNAc, shikimic acid, and PEP were purchased from Sigma. Pyruvic acid, fosfomycin, kanamycin, isopropyl-thiogalactopyranoside (IPTG), phenylmethylsulfonyl fluoride (PMSF), and benzimidazole were purchased from Bioshop Canada (Burlington, Ontario). [1-¹⁴C]pyruvate and THO (1 mCi/mL) were purchased from Amersham Bioscience, H₂¹⁸O from Cambridge.

UV/Vis spectroscopy was performed using 1cm quartz cuvettes and a Cary 100 Bio spectrophotometer. Protein purification was performed at 4 °C on an FPLC chromatographic system (Amersham Biosciences). Mini-PROTEAN 3 (Bio-Rad) was used for SDS-PAGE analysis (4% stacking gel and a 10% resolving gel) with electrode running buffer (25 mM Tris•HCl, 192 mM glycine, and 0.1% sodium dodecyl sulphate (SDS) and SDS reducing buffer (≤ 42 mM Tris•HCl, pH 6.8, ≤ 17% glycerol, ≤ 0.7% SDS, ≤ 0.07% bromophenol blue, and ≤ 3% β-mercaptoethanol). Preparative and analytical HPLC were performed using Waters 616 or 626 LC systems equipped with dual wavelength UV detectors. All liquid scintillation counting was done on a Beckman LS 6500 liquid scintillation counter. Aqueous solutions were freeze

dried using a Centrivap Concentrator (Labconco Corporation). NMR spectra were acquired on a Bruker AV 600 spectrometer. Mass spectra (MS) were collected using negative electrospray ionization (ESI) and a Micromass Quattro-LC Triple Quadrupole mass spectrometer.

2.2 Enzyme purification and compounds synthesis

2.2.1 *E. coli* MurA expression and purification

E. coli MurA were over-expressed using a pET41a (Novagen, inc.) vector in BL21*(DE3) cells (Invitrogen). In detail, a pET41a plasmid with the *E. coli* murA gene inserted between the *Bam*HI and *Nde*I restriction sites was miniprepred from an *E. coli* DH5 α preservation culture. The insert was sequenced. The murA-containing plasmid was transformed into BL21*(DE3) electro-competent cells by electroporation. LB broth (4 L) containing 30 μ g/mL kanamycin and 4% (v/v) of overnight culture was incubated at 37°C until OD₆₀₀ = 0.6. Expression was induced by 1 mM IPTG, and after a 4 hour incubation at 37°C cells were harvested by centrifugation at 5000 x g, 4°C for 10 min, yielding 3-4g/L. The pellet was then suspended in 50 mL Buffer A (50 mM Tris•HCl at pH 7.5, 1 mM EDTA, 1 mM DTT).

All the purification steps were carried out at 4°C. Just before lysing the cells, PMSF and benzamidine were added to a final concentration of

1 mM, DNase and RNase were added to a final concentration of 100 µg/mL. Then cells were lysed with a French Press for 3 passes at 10000 psi. After lysis, cell debris was removed by centrifugation at 10000 x g for 10 min. $(\text{NH}_4)_2\text{SO}_4$ was then added to 70% saturation, and precipitated protein was collected by centrifugation at 50000 x g for 10 min. The protein was then redissolved in Buffer B (Buffer A, 1M $(\text{NH}_4)_2\text{SO}_4$) by shaking for 1 h, and centrifuged again at 50000 x g for 10 min to remove insoluble precipitate. The supernatant was loaded on to a Phenyl-Sepharose High-Sub column (40 mL, Amersham Biosciences) and equilibrated with Buffer B until the absorbance returned to baseline. The protein was eluted at 5 mL/min with a gradient from Buffer B to Buffer A over 40 min. Fractions containing MurA were collected and buffer was changed to Buffer A by ultra-filtration using a YM-10 membrane. Protein was then applied to Q-Sepharose FF column (40 mL, Amersham Biosciences) and eluted in a 40 min gradient from Buffer A to Buffer C (Buffer A, 1M KCl). MurA was collected and stored at -80°C freezer. Yield was 64-76 mg/L of LB culture.

Some MurA was made PEP free, where the covalently linked PEP (phospholactoyl-enzyme adduct) was removed. To one equivalent of MurA, 2 equivalents of UDP-GlcNAc was added. After incubation for 30 min at 4°C , 8M freshly prepared urea was added to a final concentration of 6M

and the solution was shaken gently at 4°C for 2h. The urea-containing buffer was then exchanged to 1 mM DTT, 50 mM Tris•HCl at pH 7.5 by ultra-filtration using a YM-10 membrane to final urea concentration less than 0.1 mM.

2.2.2 *E. coli* AroA_{H6} expression and purification

Plasmid pET23a containing the *aroA* gene with a His6 at the C-terminal, AroA_{H6}, was transformed into BL21*(DE3) cells. The cells were grown, induced, harvested and lysed the same as MurA, except 40 mL Buffer D (50 mM Tris•HCl at pH 7.5, 300 mM NaCl, 20 mM imidazole) was used to resuspend the cell pellet. Cell debris was removed by centrifugation at 20000 x g for 30 min. The supernatant was then applied to a NiSO₄ Chelating Sepharose column (30 mL, Amersham Biosciences) at 3 mL/min. Each time, 15mL of cell lysate from 6L culture was loaded and washed with Buffer D until absorbance returned to the baseline. Buffer E (50 mM Tris•HCl at pH 7.5, 300 mM NaCl, 500 mM imidazole) was used to elute AroA_{H6}. The buffer was exchanged by ultrafiltration to 50 mM Tris•HCl at pH 7.5, 50 mM KCl, 1 mM DTT. Yield was 50 to 80mg/L of LB culture.

2.2.3 *E. coli* PPDK expression and purification

pACYC plasmid containing the pyruvate phosphate dikinase

(PPDK) gene was transformed into *E. coli* strain JM101 cells (Stratagene) by electroporation. Cells were grown up in 9L LB broth containing 20 µg/mL tetracycline and 4% (v/v) of overnight culture at 37°C. The cells were then induced, harvested, and lysed as with MurA. The protein was subjected to 50% saturated $(\text{NH}_4)_2\text{SO}_4$ precipitation, and centrifuged at 50000 x g for 10 min. To the supernatant, $(\text{NH}_4)_2\text{SO}_4$ was added to 62% saturation to precipitate PPDK, and the solution was then centrifuged at 50000 x g for 10 min. The precipitate was dissolved in Buffer F (20 mM imidazole-HCl at pH 6.4, 2.5 mM EDTA, 0.6 mM β -mercaptoethanol, 88 mM KCl), and loaded on to a DEAE-Sephadex column (~20 mL packed from 2g of dry DEAE-Sephadex resin (Amersham Bioscience)). The protein was eluted with a gradient from Buffer F to Buffer G (20 mM imidazole-HCl at pH 6.4, 2.5 mM EDTA, 0.6 mM β -mercaptoethanol, 500 mM KCl) over 40 min at 0.8 mL/min.

2.2.4 [^{14}C]PEP and [^{13}C]PEP synthesis

A 100 µL solution containing [^{14}C]pyruvate (3.67 mM, 10 µCi) or 4 mM of [^{13}C]pyruvate, 6 mM ATP, 10 mM MgCl_2 , 5 mM KCl, 5 mM Pi, 10 µM PPDK was incubated together with 10 U inorganic pyrophosphatase (PPIase) for 6 hours. After quenching by adding KOH to 200 mM and extracting with chloroform, PEP was purified by Mono-Q (Amersham Biosciences) anion exchange column with a

gradient from 10 mM NH_4HCO_3 to 500 mM NH_4HCO_3 over 30 min at pH 10.0. Large scale purifications were used for some ^{13}C PEP syntheses. The reaction mixture was purified on a 20mL Q-Sepharose column with a gradient from 250 mM to 400 mM NH_4HCO_3 at pH 10.0 over 50 min. PEP was collected and freeze-dried. Yields were typically 38% to 46% relative to pyruvate.

2.2.5 EP-UDP-GlcNAc and EPSP synthesis

Reaction mixture (up to 1mL) containing 10 mM UDP-GlcNAc (or S3P in EPSP synthesis), 10 mM PEP, 50 mM Tris•HCl, 1 μM of MurA (AroA in EPSP synthesis) was prepared and incubated at room temperature for more than 1h. After quenched with 200 mM KOH and extracting with CHCl_3 , the product was separated on a Q-Sepharose column with a gradient from 100 mM to 700 mM NH_4HCO_3 at pH 10.0 over 60 min. After the products were collected, they were freeze-dried as described in $[1-^{14}\text{C}]$ PEP synthesis. The yield for EP-UDP-GlcNAc was usually 50 to 65% and EPSP >95%.

In ^{13}C EP-UDP-GlcNAc synthesis, three-fold excess of UDP-GlcNAc was added to drive most of the ^{13}C PEP to ^{13}C EP-UDP-GlcNAc. The yield for these isotope labeled EP-UDP-GlcNAc was usually > 90% calculated relative to labeled PEP.

2.2.6 [1-¹⁴C]THI (MurA) synthesis

A 300 μ L reaction mixture containing 0.2 mM [1-¹⁴C]PEP (0.5 μ Ci), 2 mM UDP-GlcNAc, 50 mM phosphate, 50 mM Tris•HCl, pH 7.5 were prepared, and MurA was added to 2 mM and quenched within 5 seconds by 200 mM KOH. The reaction mixture was extracted with CHCl₃ repeatedly until no more protein precipitated, and then injected to Mono-Q column with a gradient from 10 mM KCl, 10 mM NH₄Cl, to 500 mM KCl, 10 mM NH₄Cl at pH 10.0 over 30 min. The yield was 14 to 25% relative to [1-¹⁴C]PEP. [1-¹⁴C]EP-UDP-GlcNAc was also purified as a byproduct and the yield was 40 to 50%.

2.3 MurA THI enzymatic breakdown

Partitioning analysis of MurA THI reaction with MurA was carried out by incubating [¹⁴C]THI with different MurA concentrations, and quenching at the same time. This reaction was coupled with two other enzymatic reactions in order to prevent any overall reaction from PEP to EP-UDP-GlcNAc. PEP was reacted with ADP to convert to pyruvate by pyruvate kinase (PK) and phosphate was consumed using by MESG with purine nucleoside phosphorylase (PNP) (Fig. 15). In detail, a 200 μ L reaction mixture was prepared containing 4.4 μ M [1-¹⁴C]THI (7000cpm), 1 mM ADP, 0.13 mM MESG, 100 mM MgCl₂, 300 mM KCl, 50 mM

Tris•HCl at pH 7.5, 0.5 U PK (Sigma), 0.3 U PNP (Sigma) and MurA (from 20 to 200 μ M) were added. The reactions were quenched after 15 to 45 min by adding 200 mM KOH and then extracting with CHCl_3 until no more protein precipitated. The quenched reaction mixture was separated by Mono-Q column with the same condition as in $[1-^{14}\text{C}]\text{THI}$ synthesis. One minute fractions were collected into scintillation vials. To each fraction, 20mL Liquiscint scintillation fluid (National Diagnostics) was added and radioactivity was counted for 2 x 5 min. The partitioning was calculated as $f(\text{PEP}) = \frac{[[1-^{14}\text{C}]\text{PEP}]}{([1-^{14}\text{C}]\text{PEP}] + [[1-^{14}\text{C}]\text{EPU}]}$, where $[[1-^{14}\text{C}]\text{PEP}]$ was calculated from $[[1-^{14}\text{C}]\text{pyruvate}]$. These experiments were conducted under different pHs. Partitioning experiments at different pHs followed the same method, except using 50 mM CAPS as buffer at pH 10.0 and 50 mM ammonium acetate at pH 5.0.

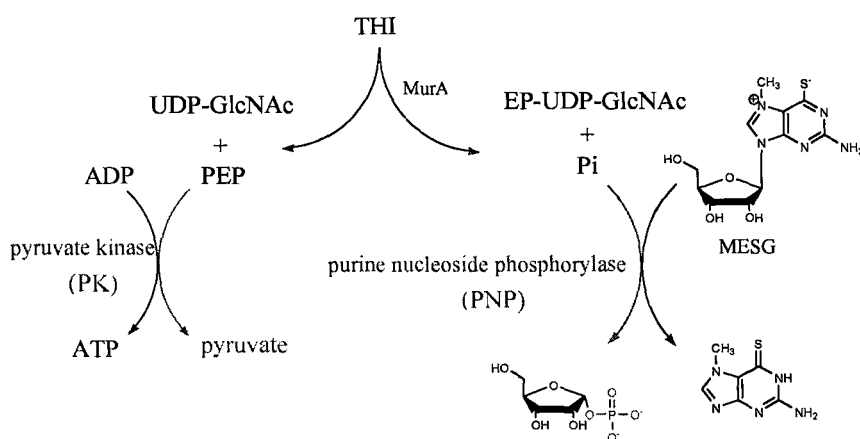


Figure 15. MurA THI enzymatic breakdown reaction. THI breakdown was coupled with PK and PNP reactions to exhaust PEP and phosphate.

2.4 Phosphate analogue/enzyme-catalyzed EP-OR hydrolysis products

2.4.1 Products characterization by HPLC

To a 200 μL reaction mixture containing 0.75 mM of EP-OR, 8.5 μM of enzyme, in 50 mM Tris•HCl at pH 7.5, arsenate was added to 40 μM . After 1h, the reaction mixture was separated by Mono-Q anion exchange chromatography as in [1- ^{14}C]THI synthesis and detected by dual wavelength UV absorbance detector at 260nm and 240nm. UDP-GlcNAc and EP-UDP-GlcNAc have different retention times and different area ratio at the two wavelengths. Under these separation conditions, S3P eluted earlier than EPSP. Standard UDP-GlcNAc, EPU, S3P, EPSP were injected and compared. Control experiments without enzyme or arsenate were done under the same conditions.

2.4.2 Products characterization by Radioactivity assay

A final concentration of 200 μM arsenate was added to 0.33 μM of [1- ^{14}C]EP-OR (with specific activity of 27mCi/mmol), 20 μM of AroA or MurA, 50 mM Tris•HCl at pH 7.5. The final volume was 100 μL . The reaction was incubated for 30 min, then separated as with [1- ^{14}C]THI synthesis, but taking 45s fractions and counting ^{14}C in each fraction.

2.4.3 Lactate Dehydrogenase reaction assay

In order to confirm that the presumed pyruvate product was indeed being formed, lactate dehydrogenase was used in a spectrophotometric assay to reduce pyruvate to lactate. Arsenate/enzyme-catalyzed EP-OR breakdown reactions were set up with 0.4 mM EP-OR, 2 mM arsenate, 0.2 μ M enzyme, 50 mM Tris•HCl, pH 7.5 in 500 μ L. After 30 min, the reaction was quenched and extracted with CHCl_3 3 times. A 10 μ L aliquot of quenched reaction mixture was analyzed by HPLC to ensure EP-OR breakdown was complete. To the remaining reaction solution, 0.1 mM NADH was added to a total volume of 1 mL in a cuvette. Lactate dehydrogenase (1 U) was added, and A_{340} was monitored.

2.4.4 Products characterization by Mass spectrometry

The products of EP-OR hydrolysis by arsenate/enzyme was identified by mass spectrometry. To a reaction mixture containing 0.5 mM EP-OR, 0.25 mM arsenate at pH 7.5, MurA or AroA was added to final concentrations of 34 μ M or 48 μ M in 100 μ L. After 5 to 28 min, the reaction was quenched with 200mM NH_4OH , followed by CHCl_3 extraction. The aqueous layer was lyophilized and analyzed by mass spectrometry.

2.5 Kinetics of phosphate analogues/enzyme-catalyzed EP-OR

hydrolysis

In order to estimate the specificity constants, k_{cat}/K_M , of phosphate analogue-promoted reactions, EP-OR was incubated with AroA or MurA, then the phosphate analogues were added to initiate the reaction. Initial rates, v_0 's, were measured and apparent k_{cat}/K_M 's were calculated using equation 1:

$$v_0 = \frac{k_{cat}}{K_M} [\text{analogue}][E] \quad (1)$$

In detail, 100 μL reaction mixture containing 333 μM of EP-UDP-GlcNAc or 750 μM of EPSP, 8.5 or 34 μM of enzyme, and 75 to 150 μM phosphate analogues, in 50 mM Tris•HCl, pH 7.5, was incubated for up to 80 min. The products were then separated by anion exchange chromatography, as above, and peaks were quantitated. For some reactions, 0.2 to 2 μM of [$1\text{-}^{14}\text{C}$]EPSP was added, and radioactivity in pyruvate and EPSP was calculated.

2.6 Mechanism of arsenate/enzyme-catalyzed EP-OR hydrolysis

2.6.1 Phosphate analogue/enzyme-catalyzed EP-OR C3 proton solvent exchange

With enzyme only, the two EP-OR ethylene protons were not

exchangeable. Solvent exchange of these protons under phosphate analogue/enzyme system was studied by incubating the reaction in D₂O.

In the arsenate/MurA-catalyzed reaction, EP-UDP-GlcNAc and arsenate were freeze dried redissolved in 190 μ L D₂O, then enzyme and volatile buffer NH₄HCO₃ at pH 7.5 were added with final concentrations of 90 μ M EP-UDP-GlcNAc, 62.5 μ M arsenate, 1.25 μ M MurA, 50 mM NH₄HCO₃ in 95% D₂O. The reaction was quenched by 50% NH₄OH at 50% completion as monitored by HPLC. The enzyme was then precipitated with CHCl₃. The aqueous layer was freeze dried and redissolved in H₂O for at least 5 times in order to exchange all the active protons in EP-UDP-GlcNAc. Finally, the mixture was dissolved in 50% MeOH/H₂O containing 2.5% formic acid and injected onto MS to analyze EP-UDP-GlcNAc isotope peaks. The vanadate/MurA-catalyzed reaction was carried out in the same way except using 225 μ M EP-UDP-GlcNAc, 125 μ M vanadate and 8.5 μ M MurA.

The solvent exchange rates of analogue/AroA-catalyzed reactions were measured by dissolving EPSP and phosphate analogues in 95% D₂O with final concentrations of 375 μ M EPSP, 25 to 333 μ M of phosphate analogue, 5.3 to 15 μ M of AroA in 50 mM NH₄HCO₃ buffer at pH 7.5. The reaction was quenched with 50% NH₄OH, 50% D₂O at different time

points varied from 1 min to 12h. After CHCl_3 extraction, the mixture was lyophilized and active protons were exchanged with H_2O . The sample was finally dissolved in 50% $\text{MeOH}/\text{H}_2\text{O}$ and EPSP isotope peaks were analyzed by MS. In the vanadate, tungstate, and sulphate containing reactions, in order to suppress any contaminant phosphate-catalyzed solvent exchange, 50 μM of KCl , 50 μM MgCl_2 , 300 μM of ADP and 0.2 U of PK were added to remove phosphate by forming ATP .

2.6.2 [$3\text{-}^3\text{H}$]EP-OR hydrolysis

In MurA -catalyzed reactions, a final concentration of 12 mM EP-UDP-GlcNAc containing 500 cpm [$3\text{-}^3\text{H}$]EP-UDP-GlcNAc, 20 mM arsenate, 40 μM MurA , 14 mM NADH , and 0.05 $\text{mg}\cdot\text{mL}^{-1}$ LDH was incubated in 50 mM $\text{Tris}\cdot\text{HCl}$ at pH 7.5. NADH and LDH were used to drive the pyruvate formed to lactate in order to prevent any tritium release from the enol form of pyruvate. A control experiment with everything except arsenate was carried out in parallel. The reactions were quenched after 15 min with 120 mM HCl and extracted with CHCl_3 three times. The aqueous solution was then diluted to 4mL and evenly divided to two scintillation vials. One vial was lyophilized by adding regular water repeatedly. Radioactivity in both the two vials was then counted for 10 min and radioactivity losses in the lyophilized vial were compared.

AroA-catalyzed reactions were followed in the same way except that 1.6 mM EPSP containing 500 cpm [$3\text{-}^3\text{H}$] EPSP, and 100 μM AroA were used, and the reactions were quenched after 6 min (100% in completion).

2.6.3 EP-OR hydrolysis in H_2^{18}O

Hydrolysis of EP-OR by arsenate/enzyme was initiated in H_2^{18}O to determine the site of nucleophilic attack by water. To a reaction mixture containing 0.5 mM EP-OR, 0.25 mM arsenate in 86 μL of H_2^{18}O at pH 7.5, MurA or AroA was added to final concentrations of 34 μM and 48 μM separately in 100 μL . After 5 to 28 min, the reaction was quenched by CHCl_3 extraction and analyzed by mass spectrometry immediately. Control experiments were carried out in the same conditions but without EP-OR or enzyme, or in H_2^{16}O .

2.7 Fluorescence titration experiments

Dissociation constants (K_d) for phosphate analogues with AroA_{H6} were determined using steady state fluorescence titrations in a 2 mL quartz cuvette at 25 °C, with 280 nm excitation wavelength and 360 nm emission wavelength. In a typical titration experiment, aliquots of 0.5 to 10 μL of ligand (phosphate or an analogue) were added to an either 0.5 or 1 μM enzyme solution in 50 mM Tris•HCl, pH 7.5, 1 mM DTT. The solution

was stirred and equilibrated for 20 min before readings (60×0.5 s) were taken and averaged. Ligand was added until no further fluorescence change was observed. After correction for dilution, fluorescence intensity was plotted versus total ligand concentration, [L], and fitted to equation 2:

$$F = F_0 - \frac{(F_0 - F_{\text{inf}}) \left\{ \frac{([E]_0 + [L] + K_d) - \sqrt{([E]_0 + [L] + K_d)^2 - 4[E]_0[L]}}{2} \right\}}{[E]_0} \quad (2),$$

where F were the observed fluorescence data, F_0 and F_{inf} were fitted fluorescence at zero and infinite [L], $[E]_0$ was the total enzyme concentration, and K_d was the fitted dissociation constant for the ligand. Titrations of the AroA mutant D313A, with EPSP and phosphate were performed the same way.

For thiophosphate and methylphosphate, the competitive inhibition of EPSP binding was also studied by fluorescence titration. In detail, different concentrations of analogue, 0.5 to 2 mM for thiophosphate and 11.5 to 115 mM for methylphosphate, were incubated with AroA_{H6} for 30 min. The mixture was then titrated with EPSP as described as before. Apparent binding constants at each analogue concentration were fitted, and K_d for each analogue was fitted to equation 3:

$$K_{d,EPSP}(\text{apparent}) = K_{d,EPSP} \left(1 + \frac{[\text{analogue}]}{K_{d,\text{analogue}}} \right) \quad (3)$$

2.8 Phosphate analogues charge calculation

The atomic charge of each deprotonated oxygen in each phosphate analogue was calculated by using the RB3PW91/6-31+G** level of theory; that is, density functional theory with Becke's exchange functional (51) and Perdew and Wang's correlation functional (52), as implemented in Gaussian 98 (53), with charges calculated using natural population analysis (NPA) (54).

3 Results

3.1 Enzyme purity, concentration and specific activity measurement

Protein purity measured by SDS/PAGE, showed >95% pure for MurA, >98% for AroA and 90% for PPDK. Enzyme identity was confirmed by DNA-sequencing, and mass spectrometry for MurA and AroA (data not shown). Protein concentrations were determined using $\epsilon_{280}=2.45 \times 10^4 \text{M}^{-1} \text{cm}^{-1}$ for MurA, $\epsilon_{280}=3.06 \times 10^4 \text{M}^{-1} \text{cm}^{-1}$ for AroA and $\epsilon_{280}=7.50 \times 10^4 \text{M}^{-1} \text{cm}^{-1}$ for PPDK, which were determined by the method of Edolhoch¹⁸. The active concentration of MurA was determined by titrating its activity with fosfomycin in a kinetic assay using Malachite Green/ ammonium molybdate to detect phosphate. It showed >90% specific activity.

E.coli MurA contained approximately 10% covalently linked PEP. In order to remove this phospholactoyl-enzyme adduct, UDP-GlcNAc was added to react with PEP. They were converted into EP-UDP-GlcNAc and phosphate. Reaction between covalently linked PEP and UDP-GlcNAc was fast. The EP-UDP-GlcNAc formed was observed 30s after UDP-GlcNAc was added after HPLC purification (Fig. 16a). Leaving the reaction too long led to EP-UDP-GlcNAc hydrolysis by the excess enzyme. The EP-UDP-GlcNAc peak can not be observed after incubation for overnight. The completion of the chasing reaction was tested by HPLC. The products

together with unreacted UDP-GlcNAc, and non-covalently linked UDP-MurNAc were removed by denaturing the enzyme with urea. By removing the urea, MurA regained 10-60% activity as compared with untreated MurA. Treated MurA was shown to be ligand free by HPLC (Fig. 16b).

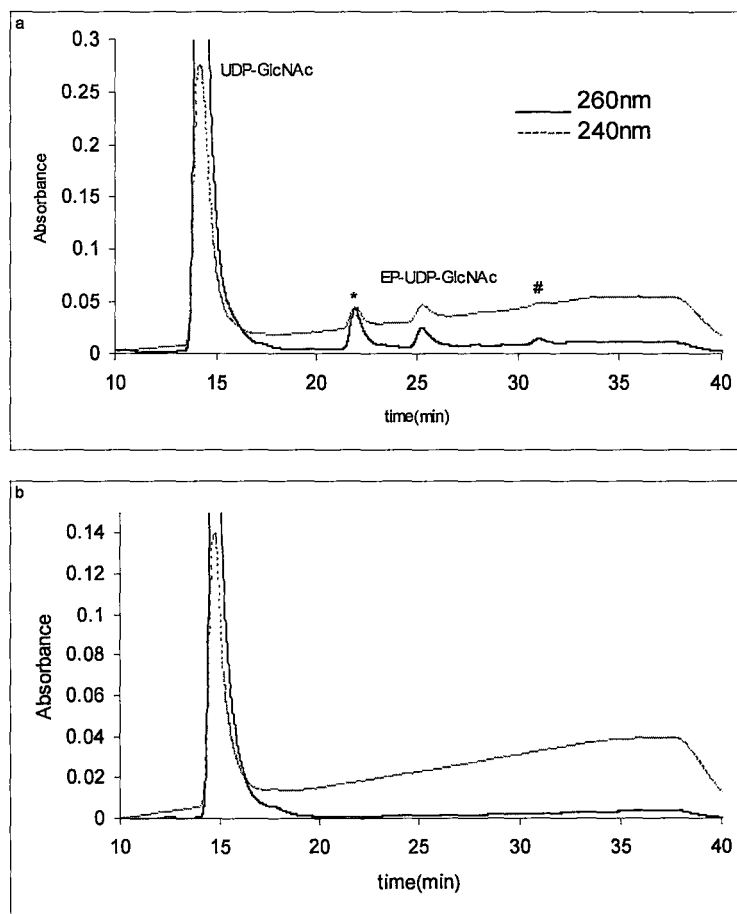


Figure 16. (a) Two equivalents of UDP-GlcNAc were added to MurA directly after purification. Covalently linked PEP was chased to EP-UDP-GlcNAc and eluted at 25.2 min. * non-covalently linked UDP-MurNAc. # MurA THI formed under excess enzyme. (b) Two equivalents of UDP-GlcNAc were added to treated PEP-free MurA. The HPLC chromatograph did not have EP-UDP-GlcNAc or UDP-MurNAc peaks showing the PEP chase was effective.

3.2 Ligands synthesis

PEP synthesis from pyruvate as catalyzed by PPDK is reversible, favouring pyruvate. Inorganic pyrophosphatase (PPiase) was added to hydrolyze inorganic pyrophosphate and drive the equilibrium forward (Fig. 17a).

EP-UDP-GlcNAc and EPSP were synthesized many times. The purification method (elution buffer concentration and gradient length) varied with injection volume and the reaction mixture (Fig. 7b, c). Concentrations of newly synthesized PEP, EP-UDP-GlcNAc and EPSP were determined by comparing HPLC peak areas with standard injection of PEP and UDP-GlcNAc. EP-UDP-GlcNAc had the same molar absorptivity as UDP-GlcNAc at 260nm. The area ratios of PEP/EPSP (determined from ^{14}C -labeled sample with same specific radioactivity) at 240nm was used to determine EPSP concentration. PEP/S3P area ratio at 240nm was measured from the reverse reaction. It was 1:0.59:2.1 for PEP:S3P:EPSP. Compound purities were 95% to 99%, as determined by HPLC. Both EP-OR's were stable at neutral and slightly basic pH (< 12) at 4°C, which is how they were stored, but not at acidic pH. EP-UDP-GlcNAc was hydrolyzed through P-O bond cleavage in 1M HCl or KOH after 2hours, yielding UMP and the other moiety (examined by MS, data not shown).

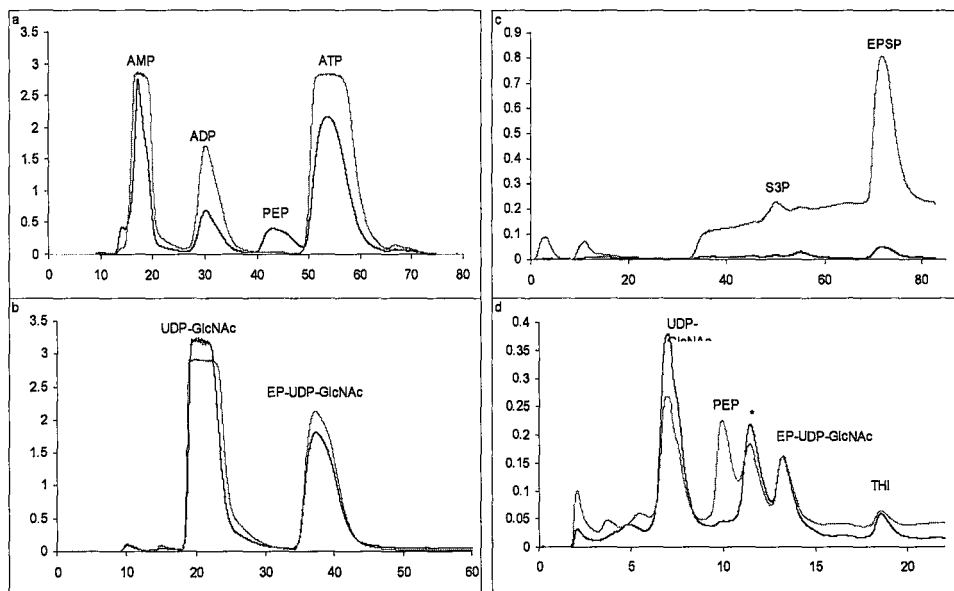


Figure 17 (a) A typical HPLC chromatogram of PEP purification on a Q-Sepharose column. (b) Labeled EP-UDP-GlcNAc purification on a Q-Sepharose column. Excess UDP-GlcNAc was used to consume all the labeled PEP. (c) EPSP purification on a Q-Sepharose column. (d) MurA THI purification on a Mono-Q column.

MurA THI is stable in basic conditions with a lifetime of 49 days at pH 12, 14 days at pH 10, and labile in acidic conditions with a lifetime of 4s at pH 4.0. Its nonenzymatic breakdown products are pyruvate, phosphate and UDP-GlcNAc. Chromatography from THI purification is shown in Fig. 17d. Identity of THI was confirmed by bringing MurA THI to pH 4.0, after 10 s bringing it back to pH10.0; then its components was examined by HPLC. Most of THI broke down to pyruvate and UDP-GlcNAc, with <5% residual THI from 260nm UV detection, which could be some impurity having the same retention time with THI (data not shown). There was no remaining radioactivity at the THI retention time when ^{14}C -labeled THI was used.

3.3 MurA THI enzymatic breakdown

The initial rate of MurA-catalyzed THI breakdown was measured. Its k_{cat}/K_m was $4 \times 10^3 \text{ M}^{-1}\text{s}^{-1}$, 3×10^4 -fold slower than AroA-catalyzed THI breakdown (30). Presumably this was due to slower binding. Trying to increase the flexibility of the active site with up to 300mM urea did not increase the reaction rate (data not shown). Higher urea concentrations led to decreasing enzyme activity, from 48% at 600 mM urea to <0.1% activity at 2 M urea. THI breakdown was slow enough that its products, [UDP-GlcNAc + PEP] and [EP-UDP-GlcNAc + Pi], would have reacted with MurA unless steps were taken to prevent this. Two coupled enzymatic reactions were used to consume PEP and phosphate, and stop any overall equilibrium reaction (Fig. 15). Pyruvate kinase (PK) is pH dependent, with lower activity at low pH (55). Large amounts were used in order to make sure all PEP can be converted to pyruvate at pH 5.0. Lower pH was not tried due to low PK activity. Initially, the purine nucleoside phosphorylase (PNP) coupled reaction with inosine failed because equilibrium favoured to Pi with equilibrium constant ~ 0.05 (56). 7-methyl-6-thioguanosine (MESG) was chosen for this reaction. MESG is not stable under basic conditions, so large amounts were used at pH 10.0, and higher pH's were not tried.

In order to accurately measure the breakdown products, at each

pH, increasing amounts of MurA were used and all reactions were quenched at the same time. Increasing amounts of each product, PEP and EP-UDP-GlcNAc, were detected. The $f(\text{PEP})$ was averaged at different enzyme concentrations. The partitioning experiments were repeated at pH 5.0, 7.5 and 10.0. As shown in Fig. 18, there is no obvious pH dependence and $f(\text{PEP})$ fluctuated from 0.20 to 0.26. The average was 0.22 ± 0.01 .

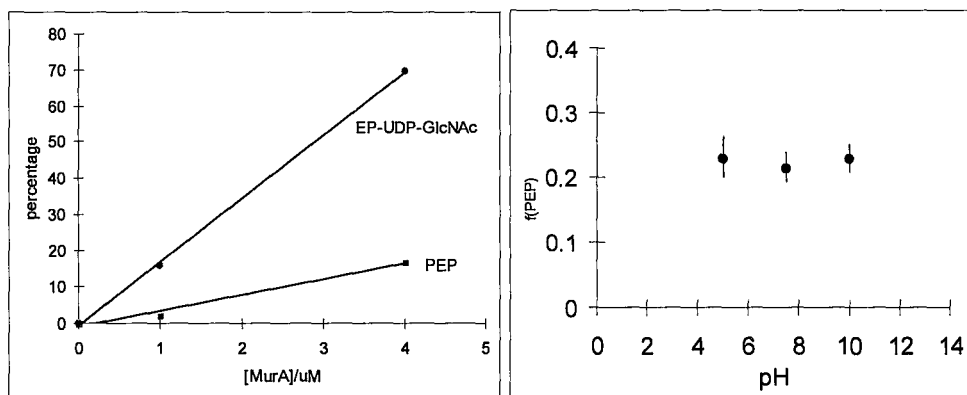


Figure 18. MurA THI partitioning versus pH. (a) Breakdown products at different MurA concentrations. (b) $f(\text{PEP})$ at different pHs.

3.4 Phosphate analogue/enzyme-catalyzed EP-OR hydrolysis products

3.4.1 Products characterization by HPLC

EP-OR was relatively stable in the presence of enzyme only, with

$k_{cat(AroA)}=4.7\times 10^{-4} \text{ s}^{-1}$, and $k_{cat(MurA)}=4.2\times 10^{-4} \text{ s}^{-1}$, compared with a literature value of $k_{cat(AroA)}=4.1\times 10^{-4} \text{ s}^{-1}$ (57), which means there would be only 1.5% of EP-UDP-GlcNAc hydrolyzed under the experimental conditions in the absence of arsenate (0.75 mM of EP-UDP-GlcNAc, 8.5 μM of enzyme, in 50 mM Tris·HCl at pH 7.5 reacted for 1h). In the presence of 40 μM arsenate, the EP-OR peak completely disappeared in anion exchange chromatograms. A new peak was eluted at the same elution time and A_{260}/A_{240} ratio as standard UDP-GlcNAc. The area ratio under dual wavelength UV detection provides a simple and fast way to identify each species in this reaction system. With a uridine ring only and no C=C bond, the area ratio of A_{260}/A_{240} for UDP-GlcNAc was ~ 1.7 . EP-UDP-GlcNAc has both uridine and C=C; its A_{260}/A_{240} ratio was 1.0. PEP with only one C=C had an A_{260}/A_{240} ratio of 0.04. A small peak at 240nm with same elution time as pyruvate was visible in enlarged chromatograms.

When arsenate was added to AroA and EPSP, and the reaction stopped before EPSP was completely hydrolyzed, S3P was observed in the HPLC chromatograph (Fig. 20).

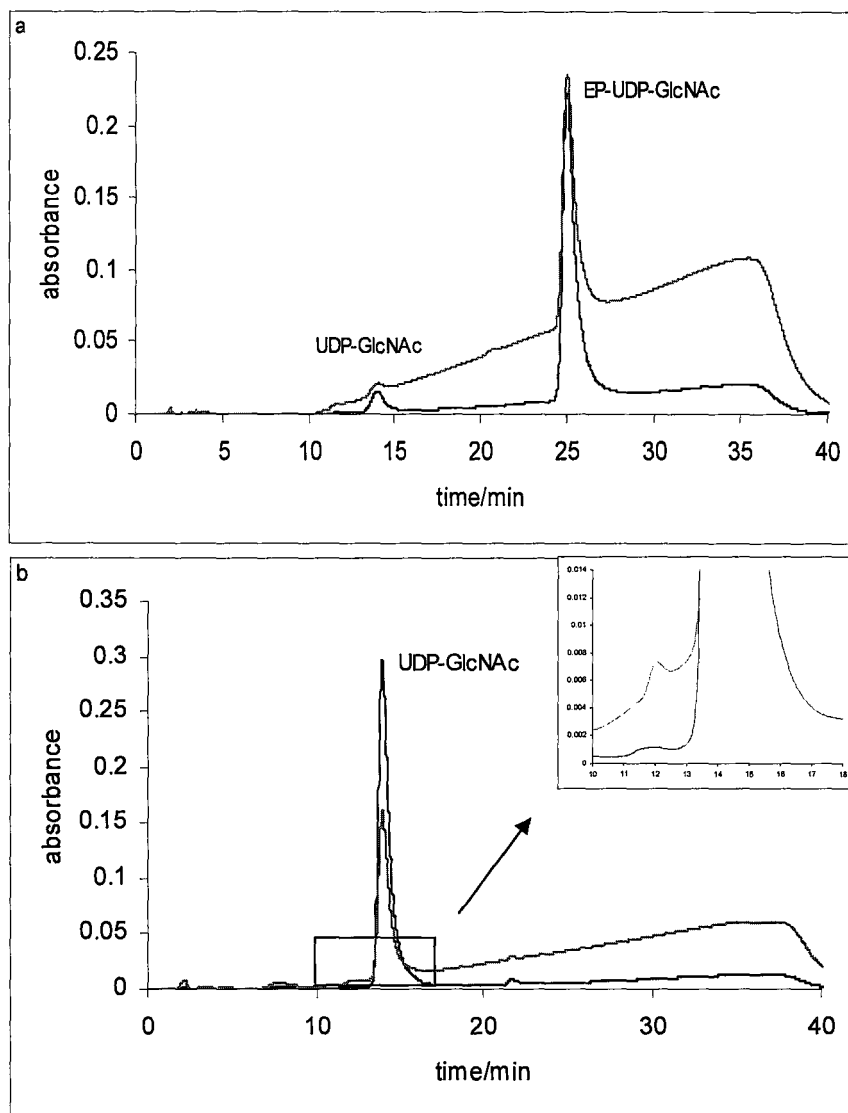


Figure 19. HPLC chromatography of arsenate/MurA-catalyzed EP-UDP-GlcNAc hydrolysis. (a) Standard EP-UDP-GlcNAc injection with contaminating UDP-GlcNAc from EP-UDP-GlcNAc synthesis. Blue line: A_{260} ; red line: A_{240} . (b) After reaction to completion, with a new peak at the UDP-GlcNAc elution time. The inset is the enlarged box area. The small peak at 13 min was believed to be pyruvate.

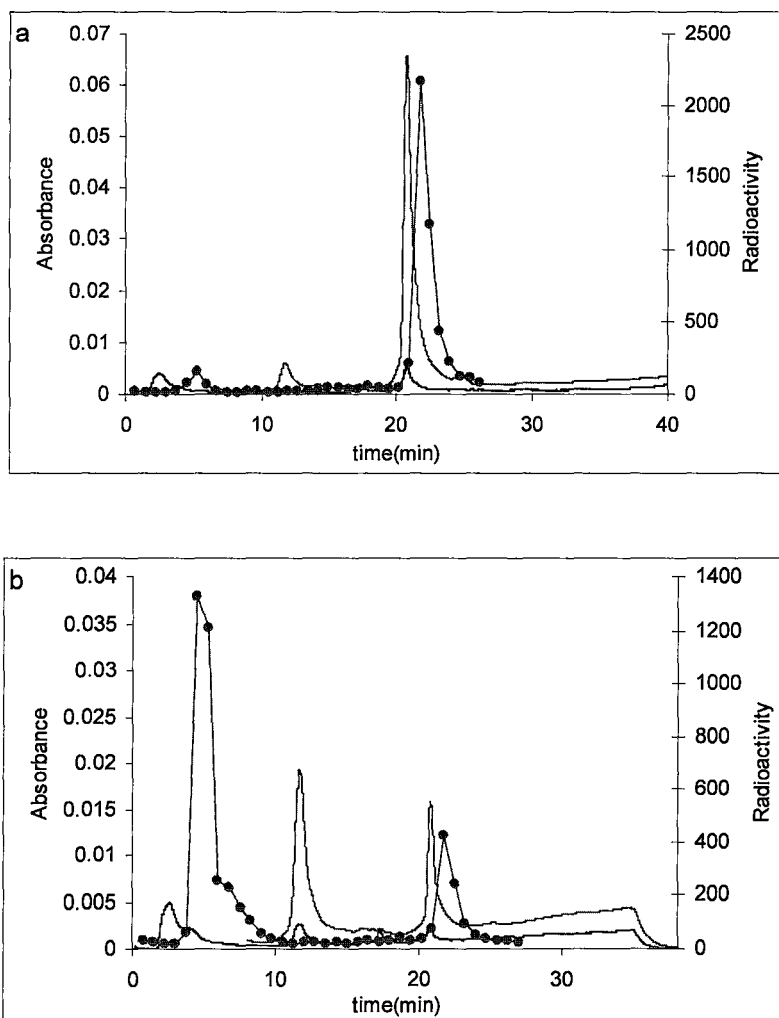


Figure 20. HPLC chromatography of AroA/arsenate-catalyzed EPSP hydrolysis. Green line, A_{240} ; blue line, A_{260} ; red line, radioactivity taken for 1 min fractions. (a) Reaction without arsenate. The small red peak at 5 min and small green peak at 12 min was contaminant pyruvate and S3P from EPSP stock solution. (b) Reaction with arsenate stopped before EPSP was completely hydrolyzed.

3.4.2 Products characterization by radioactivity assay

^{14}C labeled EP-OR was used to further identify pyruvate. Position C1 of the carboxyvinyl group was labeled with ^{14}C , so that the radioactive material would elute at the pyruvate retention time upon HPLC purification.

The results indicated pyruvate formation with MurA (Fig. 21) and AroA (Fig. 20).

The small radioactive peak at 17-18 min is believed to be PEP from covalently linked PEP in MurA (Fig. 21). The cold enzyme adduct reacted with UDP-GlcNAc and reached equilibrium with EP-UDP-GlcNAc. This experiment was performed before it became routine to treat MurA with UDP-GlcNAc and urea before experiment. There were several pieces of evidence for the formation of [1-¹⁴C]PEP. First, there was no absorbance at 260nm, and a single absorbance peak at 240nm, with elution time consistent with PEP. Second, higher MurA concentrations led to increased amounts of the putative PEP peak. When catalytic amounts of enzyme were used, the peak was very small or even disappeared. Third, when pyruvate kinase and ADP was added, the putative PEP peak disappeared, which was consistent with the reaction catalyzed by pyruvate kinase (data not shown).

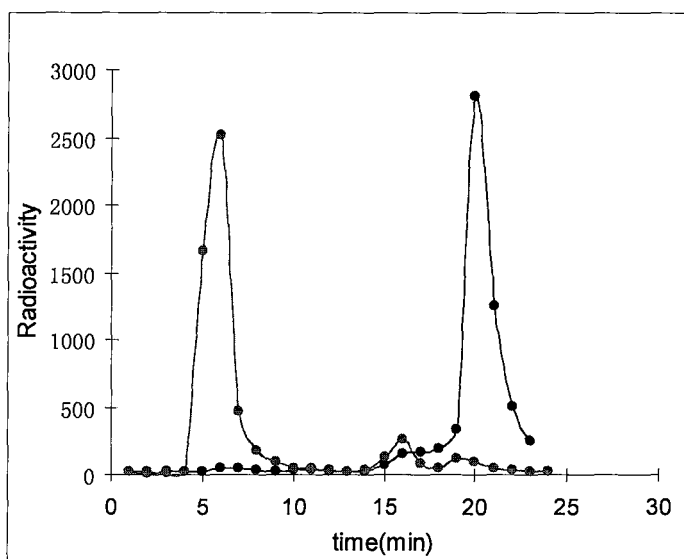


Figure 21. Evidence of pyruvate formation from EP-OR hydrolysis. The radioactivity peak shifted from EP-UDP-GlcNAc elution time (blue line) to pyruvate elution time (red line) after arsenate was added.

3.4.3 Lactate Dehydrogenase reaction assay

To further confirm one of the products was pyruvate, an enzymatic reaction was used to reduce pyruvate to lactate with NADH and lactate dehydrogenase (LDH), concomitant with A_{340} decreasing. It confirmed that pyruvate was present, with a concentration of 97 μM , compared to an expected value of 100 μM .

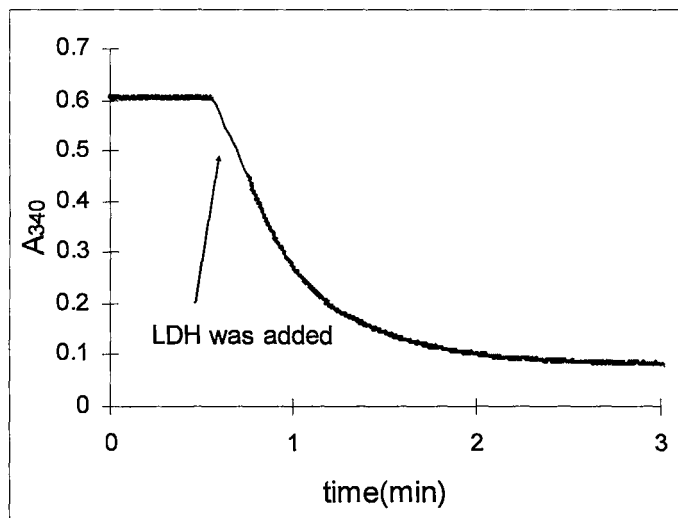


Figure 22. Evidence of pyruvate formation from LDH reaction.

3.4.4 Products characterization by mass spectrometry

To further identify the products, the reaction mixture was analyzed by mass spectrometry. Masses corresponding to UDP-GlcNAc and S3P were observed from EP-OR hydrolysis (data not shown). Pyruvate is a small molecule located in a noisy region in mass spectrum and its peak was not visible. However, from both radioactive identification and LDH coupled reaction, there was already strong evidence for pyruvate formation.

3.5 Kinetics of phosphate analogue/enzyme-catalyzed EP-OR hydrolysis

The apparent second order rate constants, k_{cat}/K_M , for phosphate

analogue-promoted EP-OR breakdown at specific EP-OR concentration were determined from the observed initial velocities. Phosphate analogue concentrations were < 4% of their K_d 's as determined by fluorescence titrations, which made it possible to estimate values of apparent $(k_{cat}/K_M)_{analogue}$ using equation 1. AroA normally follows a sequential Bi Bi mechanism with random substrate binding; we assume it follows the same mechanism when phosphate analogues were used, and in MurA-catalyzed reactions. The apparent k_{cat}/K_M approaches the true k_{cat}/K_M as EP-OR concentration become much higher than K_d 's. Under the conditions used, EP-OR concentrations (333 μ M EP-UDP-GlcNAc, 750 μ M EPSP) were much higher than K_d , which is 1 μ M for both of MurA•EP-UDP-GlcNAc (58) and AroA•EPSP (21).

Of the thirteen analogues tested, only three promoted EP-OR hydrolysis, both in MurA and AroA. They were arsenate, vanadate and fluorophosphate. Their rates were measured and compared with phosphate in the reverse reaction (Table 1). Arsenate was the most efficient analogue, only 58 times slower with AroA, and 133 times slower with MurA. This molecule was chosen for detailed study of the mechanism.

Table 1. Rate constants for phosphate-analogue promoted EP-OR hydrolysis.

	HPO ₄ ²⁻	HAsO ₄ ²⁻	HVO ₄ ²⁻	FPO ₃ ²⁻
MurA k_{cat}/K_M (s ⁻¹ μM ⁻¹)	0.02	1.5 × 10 ⁻⁴	9.4 × 10 ⁻⁵	3.3 × 10 ⁻⁶
AroA k_{cat}/K_M (s ⁻¹ μM ⁻¹)	4.5 × 10 ⁻³	7.7 × 10 ⁻⁵	2.0 × 10 ⁻⁵	1.2 × 10 ⁻⁶
Relative rate to Pi (MurA)	1	133	213	6.0 × 10 ³
Relative rate to Pi (AroA)	1	58	225	3.8 × 10 ³

3.6 Isotope labeling experiments

In order to probe the mechanism of carboxyvinyl transferases-catalyzed reactions, isotope labeling techniques were used.

Considering the low pK_a value of the EP-OR C3, one challenge for the enzyme is to protonate it into a methyl, and then deprotonate C3 back to ethylene (Fig. 23a). These unfavorable steps exist in both the forward and reverse directions. In the forward direction, incubating PEP with the enzymes does not lead to C3 protonation as there is no ³H incorporation when ³H₂O was used (27). However, this PEP C3 ethylene can be protonated in the presence of dideoxyS3P (see Section 1.4 for more detail). This indicated that binding of both substrates to the enzyme was required to generate the catalytic machinery. In the phosphate analogue-catalyzed reverse direction, C3 of EP-OR was protonated, and

was converted to pyruvate. There is no doubt that protonation occurs (Fig. 23b). The question was if there was also a deprotonation step involved. This is an important question because EP-OR breakdown without C3 deprotonation was possible, but not relevant to the true reaction. If there was a deprotonation step, what did this step contribute to the overall reaction? Is there any tetrahedral intermediate formed in the arsenate reaction that is analogous to the THI in the natural reaction?

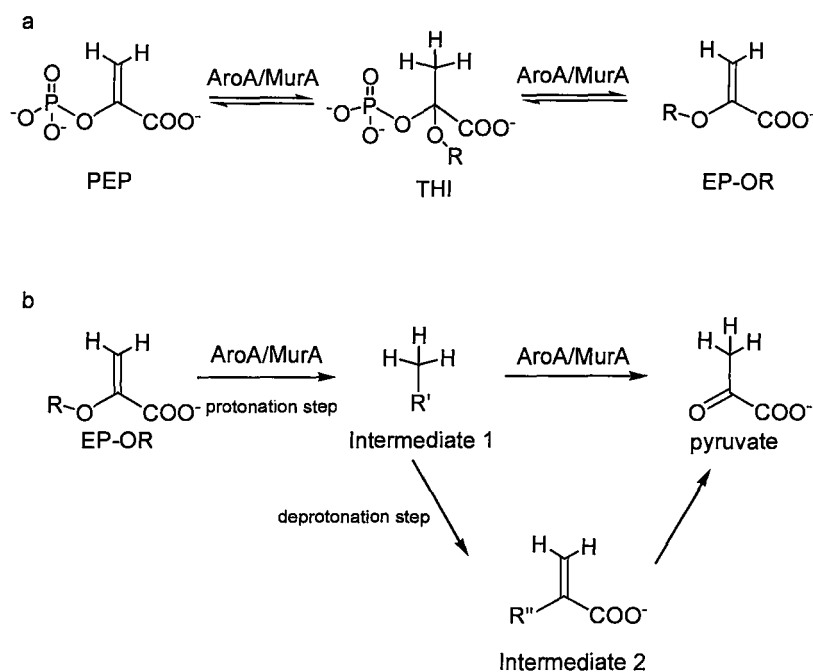


Figure 23. Reaction pathways. (a) AroA or MurA-catalyzed natural reaction. (b) Possible reaction pathways in phosphate analogue-catalyzed EP-OR hydrolysis.

3.6.1 Phosphate analogue/enzyme-catalyzed EP-OR C3 proton solvent exchange

The first experiment was designed to detect any deuterium incorporation from solvent D₂O into C3 of EP-OR. Electrospray mass spectrometry was used to monitor the formation of D-labeled EP-OR. Only D-labelling at C3 would be detected. Active protons in EP-OR could contain deuterium, in the D₂O solution, but would exchange with protium by repeatedly lyophilizing from H₂O. The D-labeled site was confirmed to be C3 by H-NMR (decreasing intensity of C3 proton signals, data not shown). Reactions were set up in volatile buffer NH₄HCO₃ in order to study by ESI mass spectrometry.

Of the thirteen analogues, arsenate, vanadate, tungstate and phosphate were chosen for this experiment. Reaction with KCl at the same concentration as analogues was used as a control.

Table 2. EPSP C3 proton solvent exchange rate compared with hydrolysis rate with AroA. nd = not detectable, nm=not measured.

	HAsO ₄ ²⁻	HVO ₄ ²⁻	WO ₄ ²⁻	SO ₄ ²⁻
AroA				
$k_{\text{ex}}/k_{\text{cat}}$	4.6	4.9	nd	nd
MurA				
$k_{\text{ex}}/k_{\text{cat}}$	6.4	0.028	nm	nm

In AroA reactions, there was no detectable [3-²H]EPSP when tungstate and sulphate were used. However, arsenate and vanadate could promote deuterium incorporation. The kinetic formation of singly and doubly labeled EPSP formation was monitored by measuring each isotope

at different time points. k_{ex} was calculated as $k_{\text{ex}} = k_{(\text{D,H-labelled})} + 2 \times k_{(\text{D,D-labelled})}$, where all the rate constants were measured for initial rate. The exchange rate was compared with hydrolysis rate as $k_{\text{ex}}/k_{\text{cat}}$ (Table 2). The D/H ratio was calculated as $\text{D/H} = (2 \times \text{D,D-labelled} + \text{D,H-labelled}) / (\text{D,H-labelled} + 2 \times \text{H,H-labelled})$, and compared with the hydrolysis rate (Fig. 24).

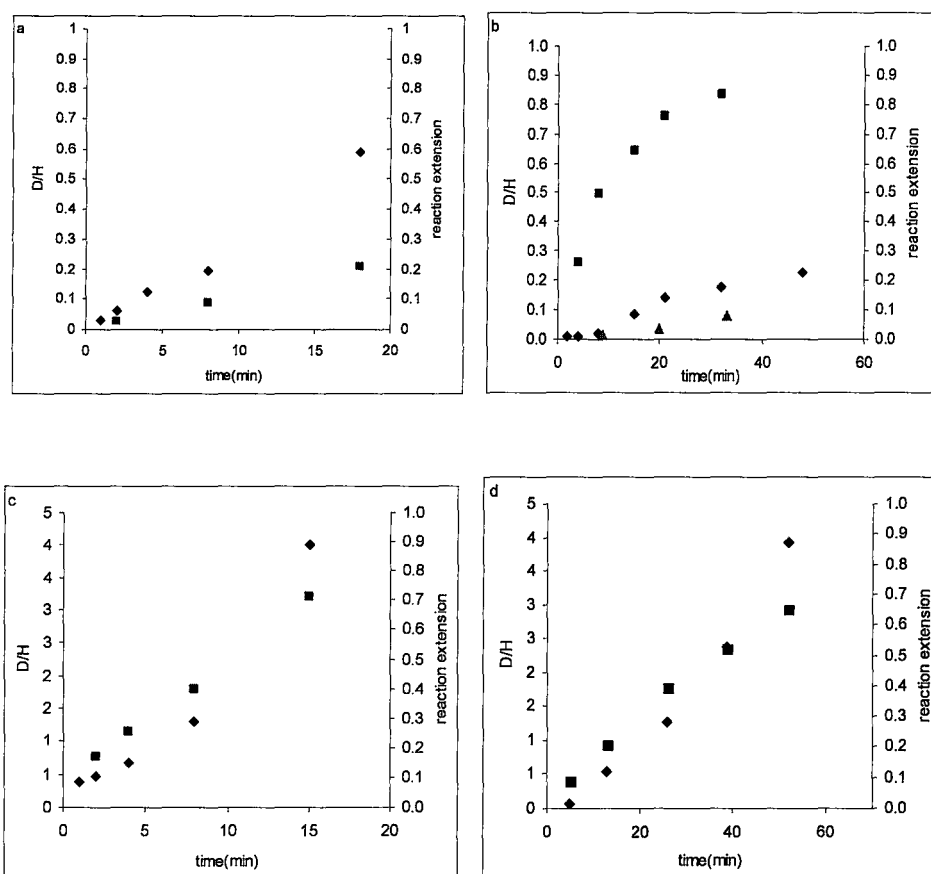


Figure 24. Phosphate analogue/enzyme catalyzed EP-OR C3 proton exchange. (a) Kinetics of EPSP proton C3 exchange and hydrolysis under arsenate/AroA. EP-OR D/H ratio is represented by (◆), and hydrolysis is represented by (■). (b) Vanadate/MurA catalyzed EP-UDP-GlcNAc hydrolysis and C3 proton exchange. (▲) represented for the EP-UDP-GlcNAc C3 D/H ratio in the control experiment under the same condition except without vanadate (c) Reaction catalyzed by Arsenate/MurA and MurA alone (d).

MurA alone catalyzed EP-UDP-GlcNAc hydrolysis showed the same $k_{\text{ex}}/k_{\text{cat}}$ ratio as in arsenate/MurA catalyzed hydrolysis, which is $k_{\text{ex}}/k_{\text{cat}}=6.3$. However this ratio is ~300 time smaller in vanadate/MurA catalyzed reaction, where after 50% of EP-UDP-GlcNAc was hydrolyzed, the D/H ratio of $[3\text{-}^2\text{H}]$ EP-UDP-GlcNAc was >2%.

3.6.2 $[3\text{-}^3\text{H}]$ EP-OR hydrolysis

Another probe of mechanism was the fate of ^3H in $[3\text{-}^3\text{H}]$ EP-OR upon reaction with MurA or AroA. ^3H will be released only if C3 is protonated then deprotonated. This would happen in reversible formation of an oxacarbenium intermediate or formation of arsenoenolpyruvate.

Deprotonation was studied by measuring tritium release from $[3\text{-}^3\text{H}]$ EP-OR. $[3\text{-}^3\text{H}]$ EP-OR was synthesized from tritium water. Due to the low specific radioactivity of tritiated water, the reaction had to be carried out parallel with a control. Tritium released from EP-OR into solvent was measured. To measure the tritium water from the reaction mixture, several methods including distillation, HPLC separation and lyophilization were tried. Among them, radioactivity loss after lyophilization gave the most sensitive and reliable results from control experiments (data not shown).

In this method, when there was no arsenate added (control), there would be no radioactivity loss before and after lyophilization. As shown in

Table 3, they were 1% for MurA and 13% for AroA reaction respectively. This could be due to contaminating tritium water from [3-³H]EP-OR synthesis. These numbers were used as background. When arsenate was added and [3-³H]EP-OR was hydrolyzed, the released tritium water was measured by comparing radioactivity in the lyophilized and unlyophilized sample. After subtracting the radioactivity loss from background, the net loss was calculated in percentage. It was 22% in MurA reaction and 20% in AroA reaction.

From ²H incorporation experiments, we expect to observe more radioactivity loss than 23%. The smaller number could be caused by a primary isotope effect on deprotonation, where deprotonate protium was much favoured than tritium. There was also some trace radioactivity left in the enzyme layer after CHCl₃ extraction. From the data, both in MurA and AroA reactions, tritium was released into the solution.

	fractional loss of ³ H ^a	
	[3- ³ H]EP-UDP-GlcNAc	[3- ³ H]EPSP
20 mM HAsO ₄ ⁼	0.23 ± 0.02	0.36 ± 0.03
no HAsO ₄ ⁼	0.01 ± 0.03	0.13 ± 0.02
fractional loss on reaction	0.22 ± 0.05	0.23 ± 0.05

Table 3. Loss of ³H from [3-³H]EP-OR upon reaction with MurA or AroA in the presence or absence of arsenate.

^a Fractional loss of ³H was calculated as the decrease in ³H between reaction aliquots which were lyophilized repeatedly from regular water after quenching the reaction, and those that were not lyophilized: fractional loss = (³H_{not lyophilized} - ³H_{lyophilized}) / ³H_{not lyophilized}.

3.6.3 EP-OR hydrolysis in H₂¹⁸O

The experiments were run in 86% H₂¹⁸O and reaction mixtures were injected directly into the electrospray mass spectrometer. Samples were not purified so as to avoid arsenate oxygen exchange with water during purification. It has been reported that at pH 8, the rate of water attack of arsenate is $1.2 \times 10^{-5} \text{ M}^{-1} \text{ s}^{-1}$ (59-61). ¹⁸O could be added to either arsenate or pyruvate, however, due to the fast hydration reaction of pyruvate under the experimental conditions, $1.0 \times 10^{-2} \text{ s}^{-1}$ at pH 7.3 (62, 63), we would expect pyruvate to contain ¹⁸O regardless of the mechanism. Thus, only arsenate peaks were monitored. Ideally, the more EP-OR in the reaction, the more cycles each arsenate molecule would be used as a catalyst, and the greater ¹⁸O incorporation that would be observed. However, the drawback of analyzing a mixture was signal depression from salt. Too much EP-OR (multiply charged) would suppress the arsenate signal. During the reaction, EP-OR concentration was chosen to be twice that of arsenate. On average, each arsenate molecule would react twice with EP-OR.

In MurA reactions without EP-UDP-GlcNAc, MurA catalyzed fast ¹⁸O exchange. Arsenate was repetitively attacked by water and isotope equilibrium was reached in arsenate oxygen after 5 min (Fig. 25a). In the presence of EP-UDP-GlcNAc, the majority was H₂As¹⁶O₄⁻. The

small amounts of ^{18}O labeled arsenate were attributed from MurA•arsenate complex rather than to reaction with EP-OR (Fig. 25b). This result indicated that most of the arsenate was in the MurA•arsenate•EP-UDP-GlcNAc, or MurA•arsenate•UDP-GlcNAc ternary complexes after the reaction, where the EP-UDP-GlcNAc protected arsenate from water attacked.

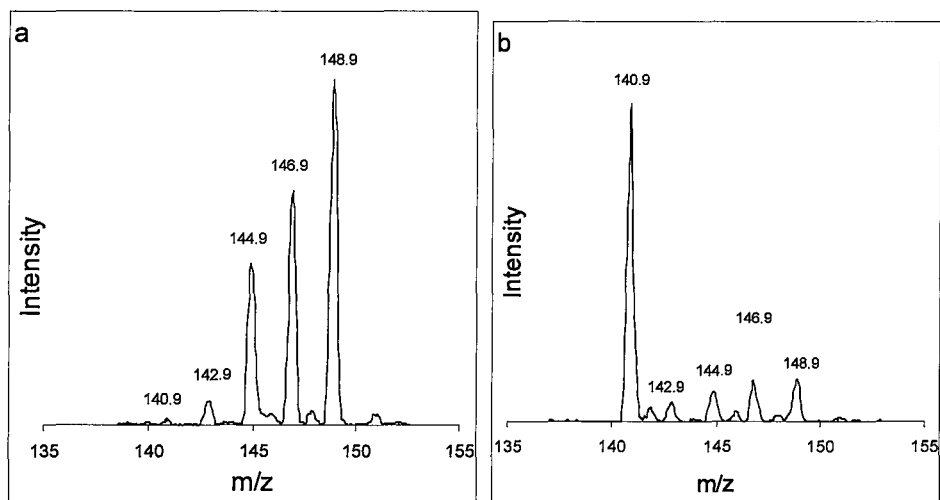


Figure 25. Mass spectra of MurA/arsenate-catalyzed EP-UDP-GlcNAc hydrolysis in H_2^{18}O . (a) MurA-catalyzed fast ^{18}O exchange in the absence of EP-UDP-GlcNAc. Reaction containing 0.25 mM arsenate, 34 μM MurA in 86% H_2^{18}O at pH 7.5 after 28 min, (b) Reaction conditions were the same as (a), except with 0.5 mM EP-UDP-GlcNAc, and the reaction was stopped after 5 min, when 70% of EP-UDP-GlcNAc was hydrolyzed.

In the AroA reaction without EPSP, oxygen exchange from water to arsenate was negligible. The exchange rate increased when EPSP was added. After $\sim 70\%$ of EPSP had been hydrolyzed, the isotope peaks $\text{H}_2\text{As}^{16}\text{O}_3^{18}\text{O}^-$ and $\text{H}_2\text{As}^{16}\text{O}_2^{18}\text{O}_2^-$ appeared with expected intensities, consistent with water attacked at the arsenic atom (Fig. 26).

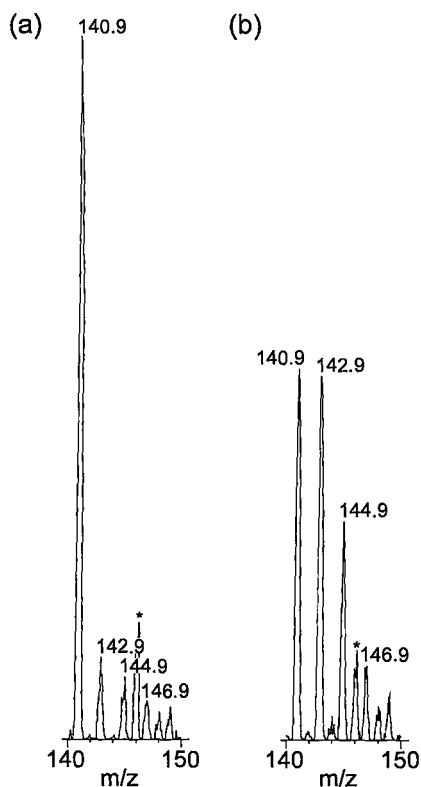


Figure 26. Mass spectra of AroA/arsenate-catalyzed EPSP hydrolysis in H_2^{18}O . (a) Reaction containing 0.25 mM arsenate, 48 μM AroA in 86% H_2^{18}O at pH 7.5 after 18 min, (b) AroA-catalyzed ^{18}O exchange during the hydrolysis of EPSP, when 70% of EPSP was hydrolyzed. Reaction conditions were the same as (a), except with 0.5 mM EPSP. * contaminant peak at m/z 145.9.

3.7 Fluorescence titration experiments

Conformational changes when ligands bound to the proteins were studied by fluorescence titration. There are two tryptophans in AroA, one located at the protein surface, and one close to the active site. When a ligand such as S3P binds to AroA, the protein undergoes a conformational change, causing an environmental change near the active centre which can be detected by fluorescence changes. This method was previously

used to study ligand binding constants and kinetics in AroA forward reaction (21).

3.7.1 Free enzyme titration

Fluorescence titrations of the free enzymes with phosphate analogues were measured. Phosphate caused AroA_{H6} fluorescence to decrease with the same titration curve as previously reported in S3P titrations (21). The value $K_{d,phosphate} = 4.8$ mM, was similar to values measured previously with wild-type AroA, which range from 0.7 mM (5) to 14 mM (64) under various conditions. Phosphate analogues that caused similar fluorescence decreases as phosphate were considered to be binding to AroA_{H6}, and K_d values were measured (Fig. 27). Vanadate absorbs at the excitation wavelength, so its binding constant was not measured. Bicarbonate and methyl phosphonic acid gave no detectable fluorescence change as compared to KCl. Sulphate cause very small changes with a different curve shape from phosphate. They were considered as not binding to AroA (Table 4).

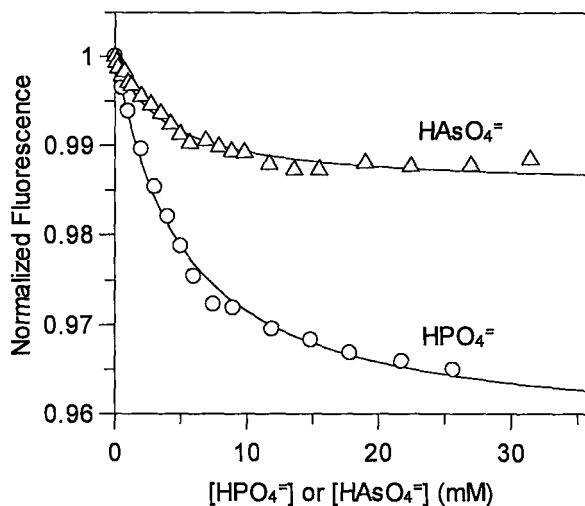


Figure 27. Fluorescence titrations of $\text{HAsO}_4^=$ and $\text{HPO}_4^=$ binding to AroA. Solid lines indicate calculated curves from fitting fluorescence data to equation 2.

Table 4. Binding constants from free AroA fluorescence titrations.

	HPO_4^{2-}	HAsO_4^{2-}	HVO_4^{2-}	FPO_3^{2-}	MeOPO_3^{2-}
K_d (mM)	4.8 ± 0.5	5.4 ± 0.6	^a	0.6 ± 0.2	23 ± 2
	HPSO_3^{2-}	WO_4^{2-}	SO_4^{2-}	MePO_3^{2-}	
K_d (mM)	0.21^b	18^c	^d	^d	

^a Vanadate strongly absorbed at the excitation wavelength, 280nm.

^b EPSP displacement titration with variable analogue concentrations.

^c Measured from phosphate inhibition constant.

^d No detectable fluorescence change up to 100 mM.

Considering the high similarity of sulphate to phosphate in terms of geometry and size, the binding of sulphate to AroA was further studied by several kinetics experiments. (1) Sulphate was added to the AroA reverse reaction mixture (phosphate + EPSP \rightarrow PEP + S3P). If sulphate could bind with AroA, it would inhibit AroA competitively with phosphate, slowing

the reverse reaction. The control experiment was conducted in parallel with KCl added to the reverse reaction in order to subtract any influence of ionic strength on AroA. Compared with KCl, sulphate did not inhibit AroA (data not shown). (2) AroA can catalyze the EPSP hydrolysis at a rate of $k_{cat} = 4.7 \times 10^{-4} \text{ s}^{-1}$. From the crystal structure, AroA has a very sterically crowded active centre. We may assume if sulphate could bind with AroA and occupy the active centre, it would prevent water molecules from approaching EPSP, thus slowing EPSP hydrolysis. The validity of this approach was demonstrated in tungstate experiments (see below). As compared with KCl, sulphate did not inhibit EPSP hydrolysis (Fig. 28).

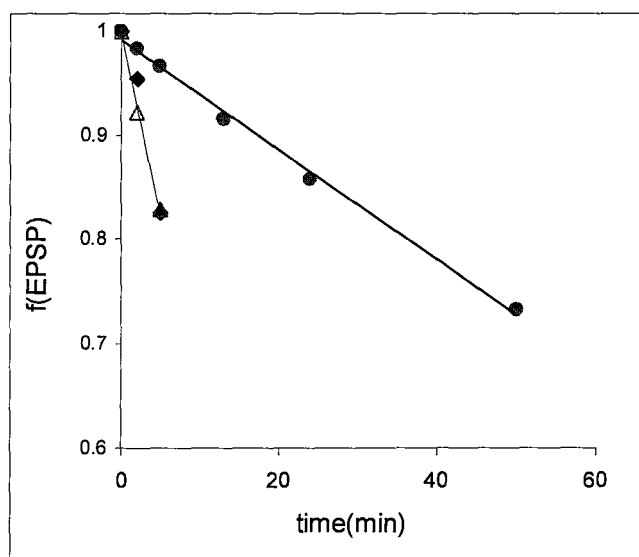


Figure 28. AroA-catalyzed EPSP hydrolysis inhibition study. To the hydrolysis reaction, 120 mM sulphate (\blacklozenge) KCl (Δ) or tungstate (\bullet) was added. $f(\text{PEP})$ is the fractional amount of EPSP remaining in the reaction mixture.

Tungstate quenches tryptophan fluorescence. Titration of AroA_{H6}

with tungstate solution gave the same titration curve as free tryptophan. Kinetic studies of the reverse reaction between EPSP and phosphate in the presence of tungstate showed tungstate was a competitive inhibitor, with $K_i = 18$ mM. In detail, the reverse reaction rate was measured with different tungstate concentrations and the rates were plotted as a function of tungstate concentration as in equation 4, where r_0 is the reverse reaction rate in the absence of tungstate, r is reverse reaction rate at [tungstate]. The binding constant was calculated from the slope.

$$\frac{1}{r} = \frac{1}{r_0} \left(1 + \frac{[\text{tungstate}]}{K_{d,\text{tungstate}}} \right) \quad (4)$$

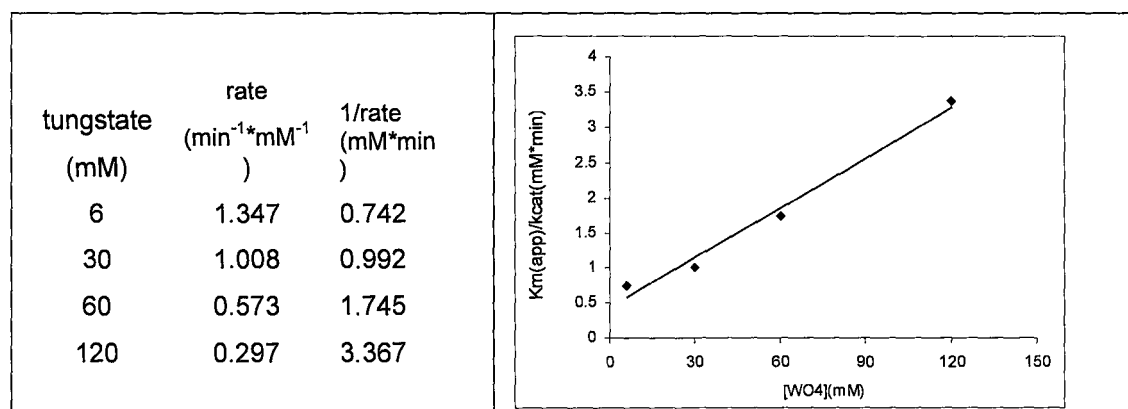


Figure 29. Tungstate inhibition of the reverse AroA reaction.

3.7.2 EPSP titration to enzyme analogue complex

EPSP binding to AroA_{H6} decreased fluorescence, and $K_{d,EPSP}$ was

measured. It was $1.6 \pm 0.1 \mu\text{M}$ compared with $1.0 \mu\text{M}$ in wild-type AroA (21). However, thiophosphate and monomethyl phosphate caused increased fluorescence when added to AroA_{H6}•EPSP complex, even though adding each ligand individually to AroA_{H6} caused decreased fluorescence. This indicated that these phosphate analogues displaced EPSP from the active site. In order to measure inhibition constant with EPSP, the apparent binding constant of EPSP ($K_{d,EPSP}(\text{apparent})$) was measured by incubating AroA_{H6} with different concentrations of these analogues, then titrated with EPSP. The displacement of EPSP by these phosphate analogues was further demonstrated by observing increased $K_{d,EPSP}(\text{apparent})$ as analogue concentration increased. $K_{d,EPSP}(\text{apparent})$ was plotted at various analogue concentrations and the $K_{i,\text{ligand}}$ for each ligand was calculated from equation 3. The inhibition constant for monomethyl phosphate was $K_{i,MeOP} = 22 \text{ mM}$, consistent with direct fluorescent titration $K_{d,MeOP} = 23 \text{ mM}$ (Fig. 30). The inhibition constant with thiophosphate $K_{i,\text{thiophosphate}}$ was 0.21 mM . Direct titration of AroA_{H6} with thiophosphate caused decreased fluorescence, but the data were hard to fit into equation 2 due to the small change in fluorescence.

To test whether monomethyl phosphate binds to AroA_{H6} in the natural phosphate binding site, rather than the site equivalent to phosphate of S3P, titration of AroA_{H6} with monomethyl phosphate was

performed in the presence of 300 μM S3P. At this S3P concentration, most of AroA_{H6} was in the $\text{AroA}_{\text{H6}}\cdot\text{S3P}$ complex form ($K_{\text{d}} = 143 \mu\text{M}$). The observed fluorescence decrease was similar to the free AroA_{H6} titration. The data was fitted to equation 2 with a binding constant of $37 \pm 3 \text{ mM}$. This was close to the monomethyl phosphate binding constant without S3P present $K_{\text{d,MeOP}} = 23 \text{ mM}$.

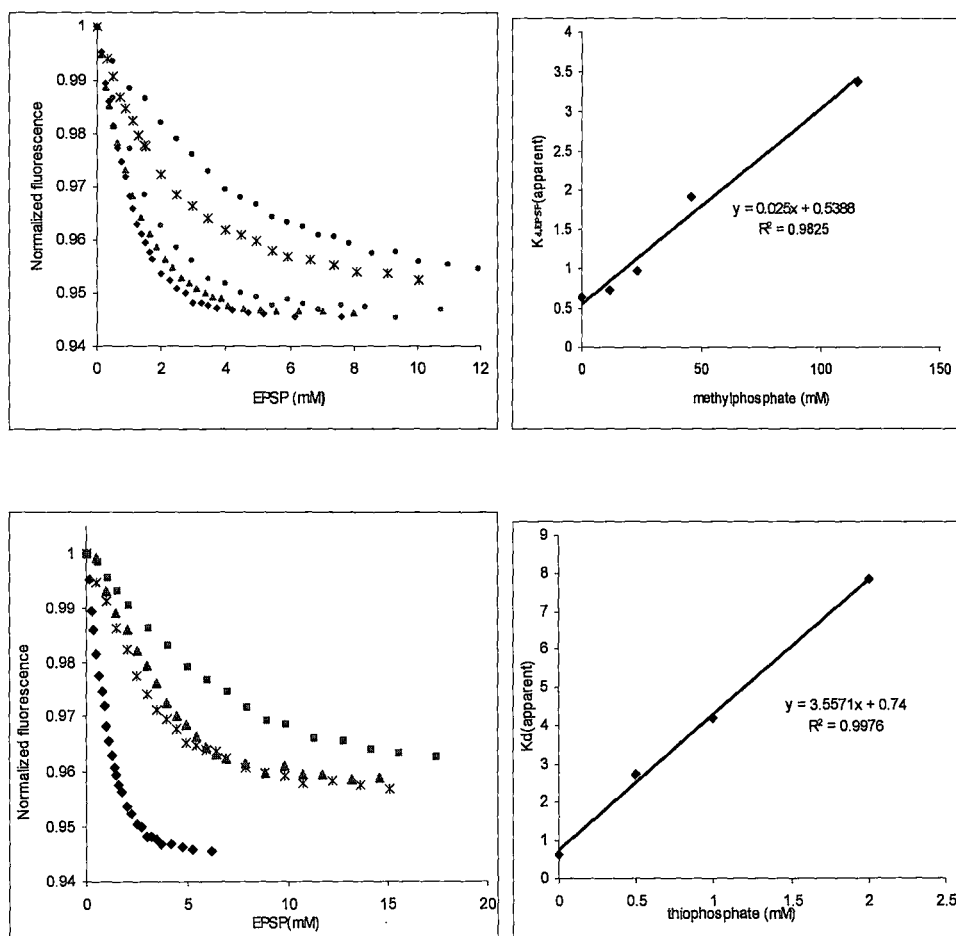


Figure 30. EPSP displacement by phosphate analogues. (a) Fluorescence titration of 1 μM AroA_{H6} by EPSP with different amounts of monomethyl phosphate: (\blacklozenge) 0 mM, (\blacktriangle) 0.5 mM, (\bullet) 1 mM, ($*$) 2 mM, (\bullet) 5 mM. (b) $K_{\text{d,EPSP}}(\text{apparent})$ as a function of monomethyl phosphate concentration. (c) fluorescence titration of 1 μM AroA_{H6} by EPSP with different

amounts of thiophosphate: (◆) 0 mM, (*) 0.5 mM, (▲) 1 mM, (■) 2 mM, d. $K_{d,EPSP(appearent)}$ as a function of thiophosphate concentration.

3.7.3 Second step titration with D313A

From all the results above, in order to promote EPSP hydrolysis reaction, phosphate analogue must bind together with EPSP in enzyme active site. To study the binding of phosphate and its analogue in the presence of EPSP, and while preventing the normal reaction, a non-reactive AroA_{H6} mutant, D313A, was used. The mutant residue D313 is far from the phosphate binding site, based on the crystal structure (33). D313A titration with EPSP or phosphate along showed similar fluorescence decays as those in AroA_{H6}, with $K_{d,EPSP} = 0.89 \mu\text{M}$ and $K_{d,phosphate} = 4.2 \text{ mM}$ respectively. Titration of EPSP-saturated D313A with phosphate caused a fluorescence decrease similar to phosphate titration of the free enzyme with the second step binding constant $K_{d,phosphate}^2 = 2.6 \text{ mM}$ (Fig. 31).

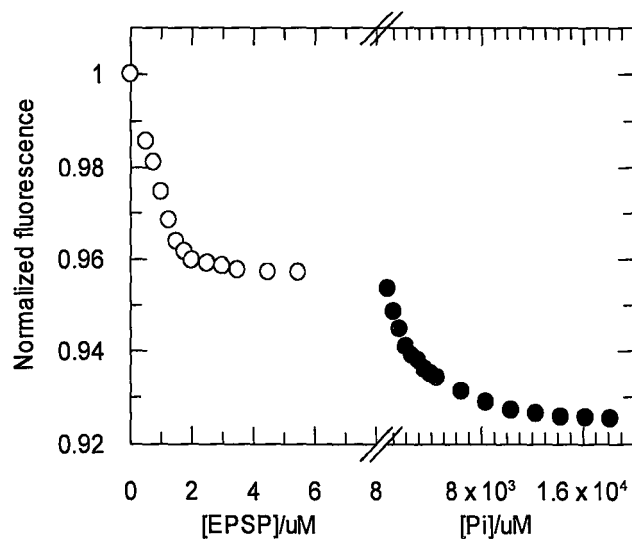


Figure 31. Fluorescence titration with D313A. D313A was first titrated with EPSP (○) and then with phosphate (●).

3.8 Phosphate analogue charge calculation

The charge on each deprotonated oxygen and the X-O bond length (X for central atom, O for deprotonated oxygen) after optimization were reported in Table 5. pK_a 's are all from the reference.

Table 5. Charge, bond length and pK_a of phosphate analogues.

	HPO ₄ ²⁻	HAsO ₄ ²⁻	HVO ₄ ²⁻	WO ₄ ²⁻	FPO ₃ ²⁻	SO ₄ ²⁻
charge on oxygen	-1.3	-1.29	-0.92		-1.27	-1.14
bond length ^f (Å)	1.5	1.66	1.68	1.77	1.49	1.48
pK _a 1 ^a	2.23	2.19			0.55	-3
pK _a 2	7.21	6.94	8.95	4.7	4.8	1.99
pK _a 3	12.32	11.5	14.4			

	MePO ₃ ²⁻	MeOPO ₃ ²⁻	HPSO ₃ ²⁻	MnO ₄ ⁻	AlF ₄ ⁻	HCO ₃ ⁻
charge on oxygen	-1.28	-1.27	-1.21			
bond length ^f (Å)	1.5	1.52	1.51			1.25
pK _a 1	2.35	1.54	<2	-2.25		
pK _a 2		6.31	5.75			
pK _a 3			10.4			

^a pK_a's from references (65-67)

4 Discussion

4.1 MurA THI enzymatic breakdown

Compared with AroA-catalyzed THI breakdown, MurA THI reacted 3×10^4 -fold slower, with k_{cat}/K_m of $4 \times 10^3 \text{ M}^{-1}\text{s}^{-1}$. Presumably this was due to slower binding because the overall catalytic efficiency of the two enzymes are similar, with MurA $k_{\text{cat}} = 5 \text{ s}^{-1}$ being only 12 times smaller than AroA $k_{\text{cat}} = 60 \text{ s}^{-1}$. The slower binding of MurA-THI may be due to lower conformational flexibility in MurA. AroA is known to undergo large-scale movements of the two domains relative to each other, while MurA only has two loops that close over the active site, but no large scale domain motions as revealed by x-ray crystallography (7).

The THI breakdown rate was so slow compared with overall reaction that chemical equilibrium would be established between the THI breakdown products, [UDP-GlcNAc + PEP] and [EP-UDP-GlcNAc + Pi], making partitioning measurement impossible without adding enzymes to consume the breakdown products before they could react again with MurA. The partitioning ratio for MurA THI breakdown was 0.22 ± 0.01 .

This coupled enzymatic reaction method was also used in other measurements. The LDH-catalyzed reaction was used to drive pyruvate to

lactate in the tritium experiment to prevent tritium release from pyruvate ketone-enol tautomerization. It was reported that the enolization reaction of pyruvate had $k=2.8\times 10^{-5} \text{ s}^{-1}$ in 50 mM Tris•HCl at pH 8.1 (62). This reaction is greatly accelerated at basic conditions with $k=0.8 \text{ s}^{-1}$ at 1M OH⁻, but it slowed in acidic conditions, so 150 mM HCl was used to quench the tritium experiments.

4.2 Mechanism of arsenate-promoted EP-OR breakdown

As arsenate was the most effective analogue at promoting EP-OR breakdown, the mechanism of the arsenate-promoted reaction was examined in detail.

AroA/arsenate catalyzed EPSP hydron exchange at C3 in ²H₂O. This implied either the formation of arseno-THI is reversible or the enzyme reversibly stabilized an oxacarbenium ion intermediate before arseno-THI formation (Fig. 32). If the newly formed methyl group rotates during the intermediate's lifetime, the catalytic base could abstract ¹H rather than the ²H that was added. ³H released from [3-³H]EPSP into solution supported this conclusion.

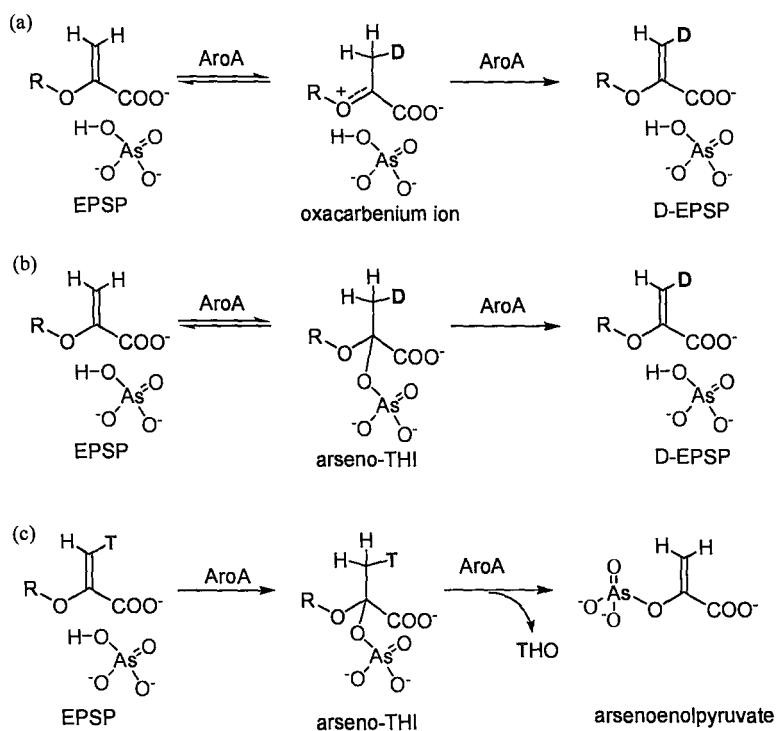


Figure 32. AroA/arsenate-catalyzed EPSP hydrolysis. (a) Possible reaction pathway for tritium release through oxocarbenium ion, where arsenate acts as a bystander. (b) Possible reaction pathway through for tritium release through reversible formation of arseno-THI. (c) Possible mechanism through formation of arsenoenolpyruvate.

In the reaction of EPSP with AroA plus arsenate in H_2^{18}O , $\text{HAs}^{16}\text{O}_3^{18}\text{O}^-$ was formed. This did not occur through direct reaction with the enzyme, as there was little ^{18}O exchange in the absence of EPSP. This indicated EPSP helped to activate arsenate for attack, presumably through arsenate ester formation. Arsenate is known to spontaneously and reversibly form arsenate esters with many hydroxyl groups (70, 71). Some enzymes such as glucose-6-P isomerase (71), accept arsenate esters as phosphate ester analogues, and catalyze to products. Usually, the products are also arsenate esters but in another form. They are then

hydrolyzed by water attacking arsenate. In AroA, the only reasonable arsenate ester forming from EPSP and arsenate was arseno-THI. This eliminates the possibility that water attacked EPSP (or the putative oxacarbenium ion intermediate) directly, with arsenate acting as a bystander.

There were two plausible mechanisms for arseno-THI breakdown. It could be released from the enzyme and hydrolyzed by water, or converted to arsenoenolpyruvate by AroA and then hydrolyzed non-enzymatically (Fig. 33). In either case, it would need to be released before pyruvate could be formed. This was consistent with the relatively flexible AroA structure, as shown by rapid THI binding, as discussed above.

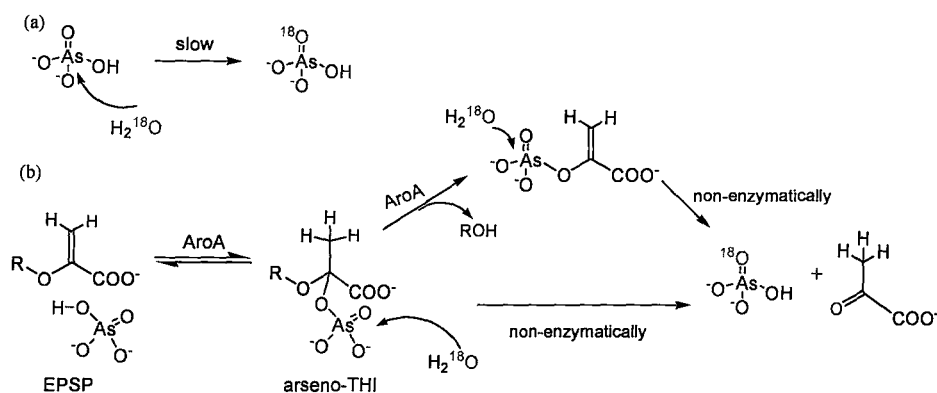


Figure 33. Mechanism of AroA arseno-THI hydrolysis. (a) H_2^{18}O attack at arsenate was slow under the experiment conditions. (b) The arsenate ^{18}O exchange was accelerated by formation of arseno-THI, which was later hydrolyzed non-enzymatically.

In arsenate/MurA-catalyzed reactions, both ^2H incorporation into

EP-UDP-GlcNAc and release of ^3H during $[3\text{-}^3\text{H}]\text{EP-UDP-GlcNAc}$ hydrolysis indicated that C3 was being protonated, then deprotonated. This would be consistent with either arseno-THI formation followed by elimination of R-OH, or with reversible arseno-THI formation, or an oxocarbenium ion intermediate (Fig 34). When there was no arsenate in presence, MurA catalyzed EP-UDP-GlcNAc hydrolysis incorporated ^2H into EP-UDP-GlcNAc with $k_{\text{ex}}/k_{\text{cat}}=6.3$ (Fig 24d). This indicated that a cationic intermediate was reversibly formed and then deprotonated (Fig 35a). When there was arsenate in presence, $k_{\text{ex}}/k_{\text{cat}}=6.4$, close to the $k_{\text{ex}}/k_{\text{cat}}$ in MurA catalyzed hydrolysis, implying there was also a reversible formation of cationic intermediate in arsenate/MurA catalyzed hydrolysis.

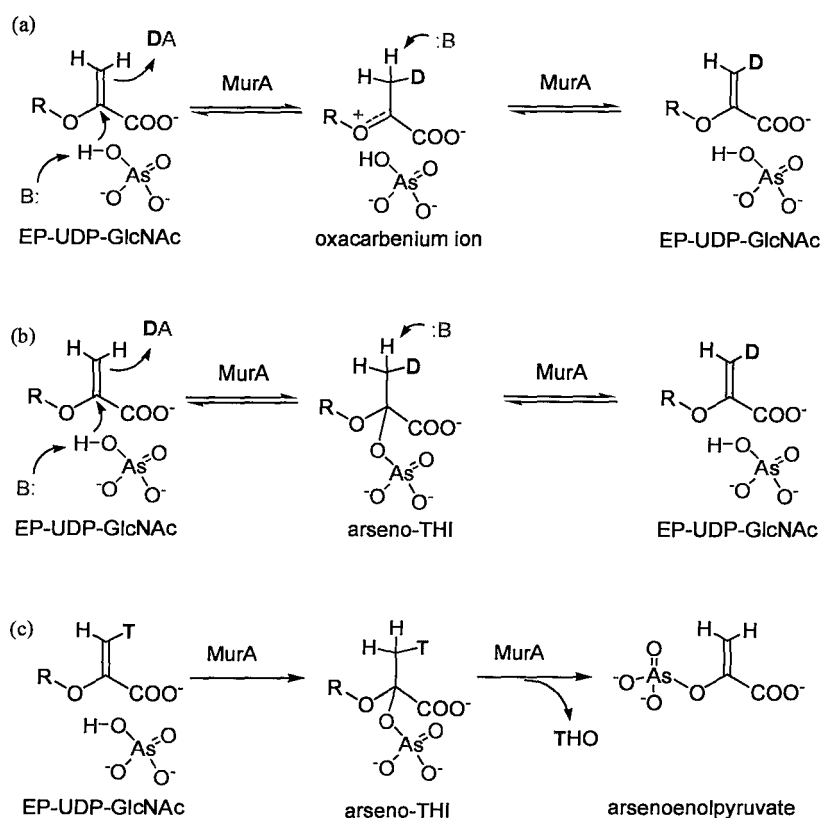


Figure 34. MurA/arsenate-catalyzed EP-UDP-GlcNAc hydrolysis. (a) Possible reaction pathway for tritium release through oxocarbenium ion, where arsenate acts as a bystander. (b) possible reaction pathway through for tritium release through reversible formation of arseno-THI. (c) Possible mechanism for MurA/arsenate-catalyzed EP-UDP-GlcNAc hydrolysis through formation of arsenoenolpyruvate.

Incubation of only MurA and arsenate in H_2^{18}O resulted in complete exchange of the arsenate oxygens, reaching equilibrium with the solvent within 5 min. However, addition of EP-UDP-GlcNAc resulted in formation of pyruvate with minimal ^{18}O exchange into arsenate. This indicated that water attacked the C2 position of arsenoenolpyruvate rather than arsenic.

There was no direct evidence of arseno-THI formation. It is possible for the arsenate to act as a bystander to induce a cationic intermediate EP-UDP-GlcNAc, and then attacked by water directly (Fig 35b). However, based on the similarities to the AroA reaction and the structural similarity of phosphate and arsenate, it is more likely for the arsenate/MurA catalyzed reaction undergoing the similar reaction pathway, through formation of arseno-THI and then arsenoenolpyruvate. The normal pathway of arsenate ester breakdown in water is through As-O bond cleavage (68, 69). The lack of ^{18}O incorporation into arsenate in the arsenate/MurA catalyzed reaction was somewhat unexpected and could indicate arsenoenolpyruvate breakdown through either an arsenolactoyl adduct, analogue to the commonly observed phospholactoyl adduct, or by MurA-catalyzed water attack on C2 of arsenoenolpyruvate. (Fig. 35c).

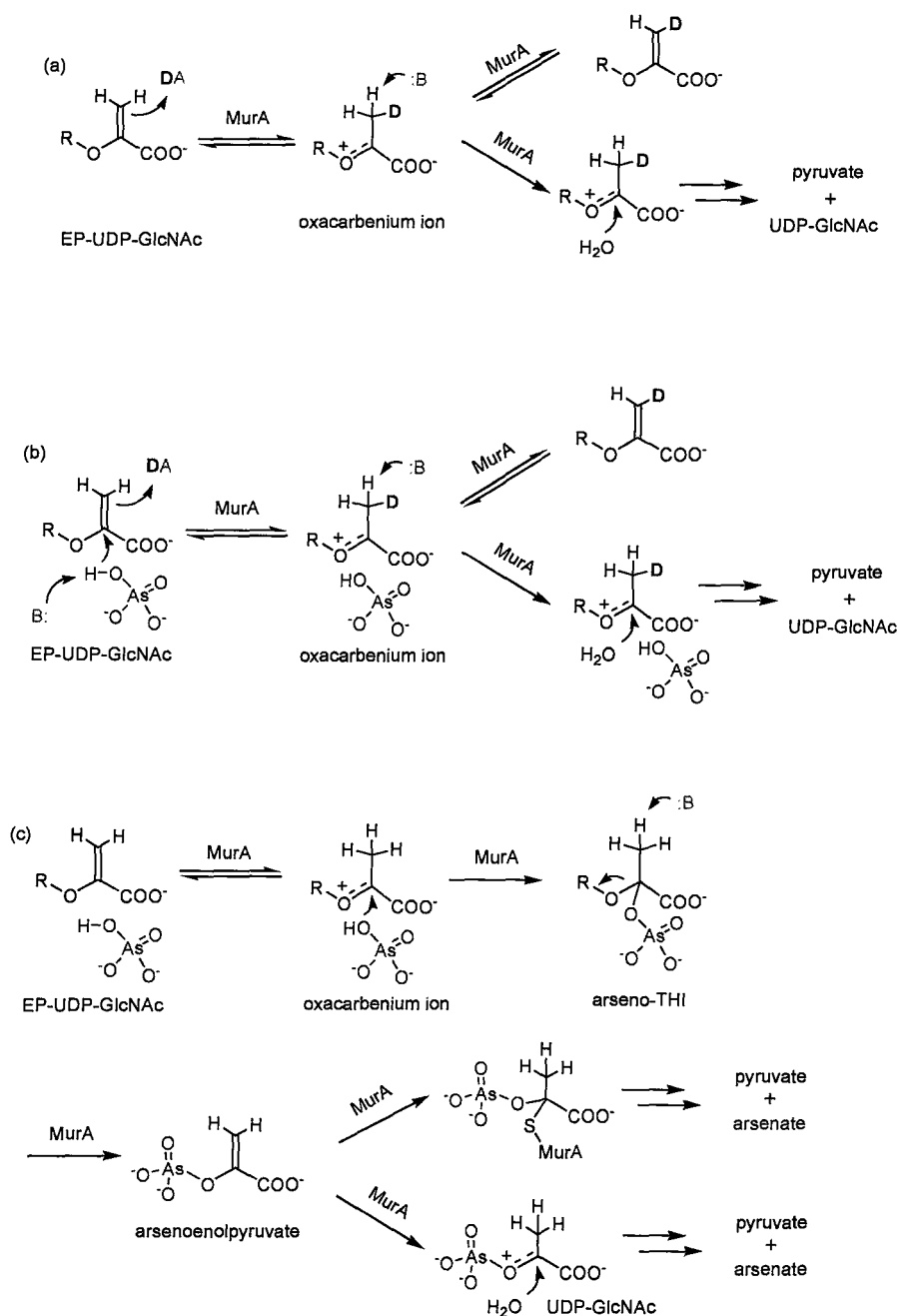


Figure 35. Proposed mechanism of EP-UDP-GlcNAc hydrolysis. (a) Mechanism of MurA catalyzed EP-UDP-GlcNAc hydrolysis. (b) Possible mechanism of arsenate/MurA catalyzed reaction through water directly attack. (c) Possible mechanism of arsenate/MurA catalyzed reaction through arseno-THI formation.

Vanadate/MurA catalyzed EP-UDP-GlcNAc showed very little ^2H

incorporation into C3. It made the first step, formation of cationic intermediate or arseno-THI, almost irreversible. The ^3H release experiment and ^{18}O incorporation experiment have not been studied yet. Because of the less ^2H incorporation, these experiments could reveal more information about the mechanism.

4.3 Oxacarbenium ions

In arsenate/MurA-catalyzed EP-UDP-GlcNAc breakdown, arsenoenolpyruvate was enzymatically hydrolyzed at a less favoured site. This could only happen when the enzyme made nucleophilic attack at C2 carbon more favourable than at arsenic, such as the enzyme distorting arsenoenolpyruvate to have oxacarbenium ion character. It was reported previously that AroA could catalyze hydron exchange in PEP in the presence of dideoxyl-S3P (27) (Fig. 4). This likely arises from transient oxacarbenium ion formation. It is reasonable for MurA to stabilize a similar structure, oxacarbenium ion-like arsenoenolpyruvate (Fig. 36), thus making C2 more electrophilic than arsenic. This work contributed another piece of evidence for oxacarbenium ion mechanism in the first step of MurA-catalyzed natural reaction.

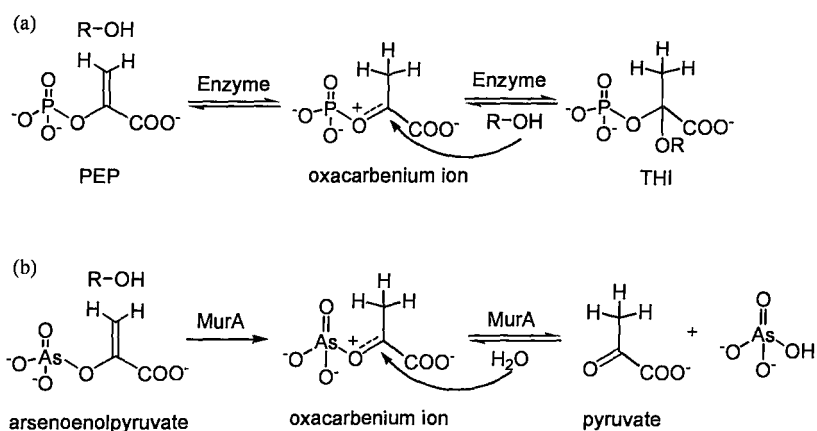


Figure 36. (a) Mechanism of the first step of the natural reaction. An oxacarbenium ion of PEP is formed and attacked by an alcohol in each enzyme. (b) The proposed mechanism of arsenoenolpyruvate hydrolysis, through a similar transition state as in (a), an oxacarbenium ion.

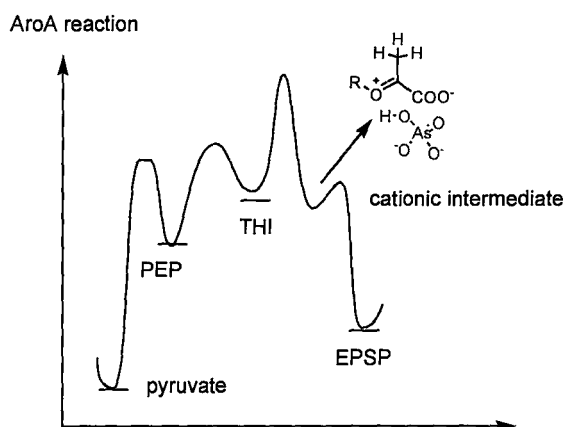


Figure 37. Reaction coordinate in AroA/arsenate-catalyzed EPSP hydrolysis reaction.

In arsenate/enzyme catalyzed EP-OR hydrolysis, the observation that the solvent exchange rate was 5~7-fold faster than hydrolysis implied that arseno-THI formation and/or oxacarbenium ion were reversible. The THI partitioning studies showed EP-OR formation was favoured over PEP + alcohol by only 2.5 and 3-fold in MurA and AroA reaction respectively.

This indicated that there is another reversible step between arseno-THI and EP-OR, that is, cationic intermediate (Fig. 37). Another study from our lab demonstrated AroA-catalyzed ketal formation, giving another piece of evidence for this cationic intermediate (72). So the overall reaction pathway for AroA/arsenate-catalyzed EPSP hydrolysis was mapped in Fig. 38.

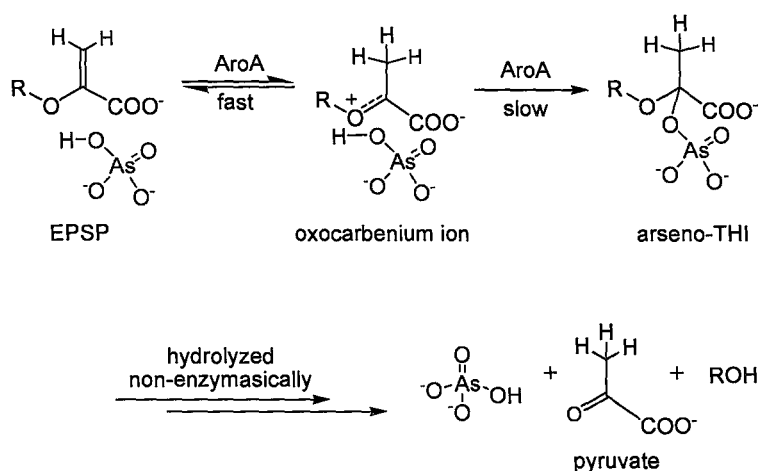


Figure 38. Reaction pathway for AroA/arsenate-catalyzed EPSP hydrolysis

PEP and EP-OR are stable in solution; protonation of carbon bases is difficult both thermodynamically and kinetically. Acid-catalyzed EPSP hydrolysis is through rate-limiting protonation at C3 to form a transient oxocarbenium ion intermediate. At 25 °C, pH 0, $t_{1/2} \approx 12$ h for this reaction (73). In contrast, both AroA and MurA can catalyze their reactions with $t_{1/2} < 0.15$ s at neutral pH and 25 °C. This impressive catalytic power is not expressed as soon as EP-OR binds to the enzyme. It is essentially

unreactive in the absence of the second substrate, phosphate. Phosphate is an intrinsically poor nucleophile. Evidence from arsenate/AroA-catalyzed EPSP hydrolysis indicates the enzyme promotes the reaction by stabilizing an oxacarbenium ion(-like) structure, which is most likely the mechanism in the natural reverse reaction. The mechanism of MurA-catalyzed reaction is under investigation by kinetic isotope effects analysis.

4.4 Phosphate analogue binding pocket

Aside from the natural phosphate binding site, phosphate could also bind to AroA in the site equivalent to the phosphate of S3P. The same titration was performed with a non-reactive mutant AroA, D313A, where D313 was located far from both phosphate binding sites. Titration of D313A with phosphate gave similar fluorescence decrease as in AroA_{H6} titration, with a slightly smaller K_d of 4.2 mM. This implied D313A did not destroy the phosphate binding site. This experiment was repeated in the presence of 2 μ M EPSP ($2 * K_d$), where most of the enzyme were bonded with EPSP. There is no significant difference except for a smaller K_d of 2.6 mM, which was also consistent with a tighter binding in the second step when EPSP is present (64). This indicated EPSP did not interfere with phosphate binding, supporting the conclusion that phosphate bound that in the normal site when titrated in the absence of EPSP, as did

arsenate (data not shown).

Titration of AroA_{H6} with monomethyl phosphate was compared to that in the presence of 300 μM S3P ($K_d = 143 \mu\text{M}$). The result was $37 \pm 3 \text{ mM}$, close to the monomethyl phosphate binding constant without S3P present ($23 \pm 3 \text{ mM}$). This implied that that larger ligand, monomethyl phosphate, also bound to the same site as normal phosphate. This conclusion is also supported by the observation that monomethyl phosphate interfered with EPSP binding (see results in 3.7.2).

4.5 Two conformational changes upon substrate binding

The second binding step was also studied by fluorescence titration. It is widely believed that both MurA and AroA-catalyzed reactions involve an induced-fit mechanism in the forward reaction (8, 74), where addition of UDP-GlcNAc to free MurA and glyphosate to AroA·S3P complex generate protein conformational changes. However, little attention was paid to the reverse reaction. Fluorescence titration of free AroA with phosphate indicated a conformational change as phosphate bound to AroA. To probe how phosphate and phosphate analogues behaved when there was EPSP in the AroA active centre, phosphate and arsenate were used to titrate the AroA·EPSP complex. The fluorescence change upon EPSP binding was followed by a second fluorescence change upon phosphate or arsenate

binding, providing evidence for a second conformational change. In the absence of phosphate or an effective analogue, binding of EPSP to AroA could not generate an enough conformational change to efficiently induce cationic intermediate formation. It has to bind with phosphate to induce a second conformational change, by which the enzyme stabilizes the oxacarbenium ion intermediate to active the nucleophilic attack (Fig. 39). Analogues that could not promote the reaction, such as sulphate, also could not induce the second conformational change as shown from fluorescence experiments.

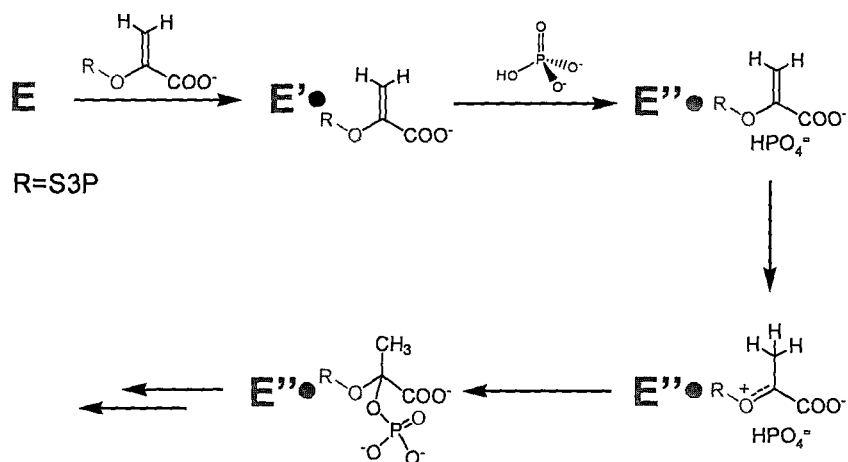


Figure 39. Proposed mechanism for AroA-catalyzed reaction. E represents for enzyme AroA, different color represents for a different conformational state. The second conformation was needed to stabilize an oxacarbenium ion EPSP in the reverse reaction.

4.6 Phosphate analogues

Of the four molecules that could promote reaction, all are tetrahedral, and three had a charge of -2, and are protonated at

physiological pH, *i.e.*, $\text{HPO}_4^{=}$, $\text{HAsO}_4^{=}$, and $\text{HVO}_4^{=}$. The exception was $\text{FPO}_4^{=}$, which is 0.2% protonated at physiological pH. The lower activity with $\text{FPO}_4^{=}$ could be due to the low concentration of HFPO_4^- at physiological pH. $\text{WO}_4^{=}$ with 99.8% deprotonated and -2 charged at physiological pH was able to compete with phosphate for binding but unable to promote breakdown or solvent exchange. The problem may be size, with W-O bond lengths of 1.77 Å compared with 1.50 Å for $\text{HPO}_4^{=}$. As implied by the results, tungstate bound at the phosphate site and expelled both phosphate and EPSP out of active centre. Similarly, $\text{HPSO}_3^{=}$ with a P-S bond length of 2.13 Å could displace EPSP from catalytic centre (Fig. 40). Monomethyl phosphate $\text{H}_3\text{C-OPO}_3^{=}$ had one larger functional group, the methoxy, and interfered with EP-OR binding, presumably because the methyl group occupied part of the space occupied by EP-OR. Displacement of EPSP by $\text{HPSO}_3^{=}$ and $\text{H}_3\text{C-OPO}_3^{=}$ was consistent with previous observation in the crystal structures of AroA that its active site was very constrained.

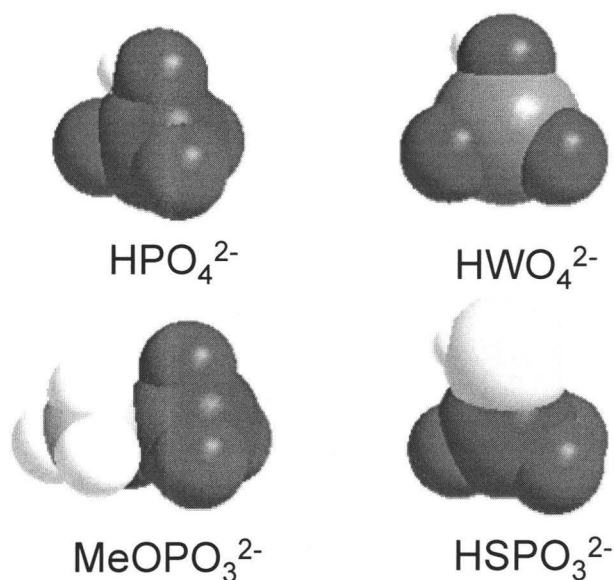


Figure 40. Models of phosphate and “big” phosphate analogues. All the models are from computational calculation (see experimental procedure).

In many ways, the closest phosphate analogue was sulphate, in terms of its tetrahedral geometry, size and overall charge. However, as demonstrated by competitive inhibition and several other experiments, including deuterium solvent exchange, sulphate did not bind to AroA. The major difference between HPO_4^- and SO_4^- is the lack of a proton on sulphate at physiological pH. This distinction may be important physiologically. Bacteria actively import sulphate, with intracellular SO_4^- concentrations around $100 \mu\text{M}$ (75). It would be expected that enzymes would have a means to distinguish between sulphate and phosphate. It has been proposed that the lack of a proton in SO_4^- is the main way that proteins distinguish between sulphate and phosphate (76). Now the question is how the enzyme evolved itself to discriminate

one single proton. An unexpected result from AroA mutation studies was a single mutation D49A decreased AroA_{H6} activity by 21000-fold (30). Based on crystal structures, except for the presumed catalytic base E341 in AroA and C115 in MurA, which was used to deprotonate C3 hydrogen, D49 is the only negatively charged residue around phosphate. This residue is 100% conserved in both AroA and MurA (30). The enzymes use several hydrogen bond donor residues (K22, R100, R124, Q171 in AroA and K22, R91, R120 in MurA) to stabilize negative charge on phosphate oxygens. The role of a hydrogen bond acceptor residue, D49, and why it was so important to catalysis is not well understood. However, it would not too surprising if the enzymes used this residue to form a strong hydrogen bond in order to differentiate phosphate from sulphate.

Among all the phosphate analogues, only those that could bind to the enzyme together with EPSP could promote the reaction. Analogues that could not bind together with EPSP could not catalyze solvent exchange either. This implied the enzyme needed the second ligand to bind, which helped to stabilize the oxacarbenium ion like form of EPSP, and then make C3 proton exchangeable and C2 electrophilic.

5. Conclusions

Thirteen different phosphate analogues were used to study the reverse reactions of AroA and MurA from EP-OR. Among these phosphate analogues, many could bind to the free enzyme, but only three could promote hydrolysis.

The products from EP-OR hydrolysis were pyruvate and the corresponding alcohol (S3P in the AroA/EPSP reaction and UDP-GlcNAc in the MurA/EP-UDP-GlcNAc reaction). The most effective analogue was arsenate. The mechanism of the arsenate-promoted reaction was examined in detail. Based on ^{18}O , ^2H and ^3H isotope labeling experiments, hydrolysis proceeded through an arseno-tetrahedral intermediate with AroA, a similar reaction pathway to the natural reaction. This arseno-tetrahedral intermediate was converted to arsenoenolpyruvate and degraded spontaneously in water through As O bond cleavage. MurA also likely catalyzed arseno-tetrahedral intermediate formation, and appeared to catalyze arsenoenolpyruvate breakdown, though it is possible that it was a bystander in the reaction, with the tetrahedral intermediate being formed by water attack on C2 of EP-UDP-GlcNAc.

The catalytic machinery for stabilizing such as unstable oxacarbenium ion like intermediate was investigated. Based on information from all the phosphate analogues, in the AroA-catalyzed

reverse reaction, there was evidence that AroA undergoes an conformational change upon binding with phosphate, which the protonated form of EPSP was stabilized. This was consistent with the fact that only those who can bind together with EP OR were able to generate an effective second conformational change, thus promoting EP OR breakdown and solvent deuterium incorporation into the C3 ethylene group.

6. References

1. Bugg, T. D., and Walsh, C. T. (1992) *Nat. Prod. Rep.* **9**, 199-215.
2. Gunetileke, K. G., and Anwar, R. A. (1968) *J. Biol. Chem.* **243**, 5770-5778.
3. Walsh, C. T., Benson, T. E., Kim, D. H., and Lees, W. J. (1996) *Chem. Biol.* **3**, 83-91.
4. Schmid, J., and Amrhein, N. (1999) *The shikimate pathway. In Plant Amino Acids: Biochemistry and Biotechnology, Marcel Dekker: New York,* 147-169.
5. Anderson, K. S., and Johnson, K. A. (1990) *Chem. Rev.* **90**, 1131-1149.
6. Anderson, K. S., Sammons, R. D., Leo, G. C., Sikorski, J. A., Benesi, A. J., and Johnson, K. A. (1990) *Biochemistry* **29**, 1460-1465.
7. Schonbrunn, E., Sack, S., Eschenburg, S., Perrakis, A., Krekel, F., Amrhein, N., and Mandelkow, E. (1996) *Structure* **4**, 1065-1075.
8. Schonbrunn, E., Svergun, D. I., Amrhein, N., and Koch, M. H. (1998) *Eur. J. Biochem.* **253**, 406-412.
9. Brown, E. D. V., E. I.; Walsh, C. T.; Kolter, R. (1995) *J. Bacteriol.* **177**, 4194-4197.
10. Marquardt, J. L., Brown, E. D., Lane, W. S., Haley, T. M., Ichikawa, Y., Wong, C. H., and Walsh, C. T. (1994) *Biochemistry* **33**, 10646-10651.
11. Kim, D. H., Lees, W. J., Kempell, K. E., Lane, W. S., Duncan, K., and Walsh, C. T. (1996) *Biochemistry* **35**, 4923-4928.
12. Steinrucken, H. C., and Amrhein, N. (1984) *Eur. J. Biochem.* **143**, 351-357.
13. Roberts, F., Roberts, C. W., Johnson, J. J., Kyle, D. E., Krell, T., Coggins, J. R., Coombs, G. H., Milhous, W. K., Tzipori, S., Ferguson, D. J., Chakrabarti, D., and McLeod, R. (1998) *Nature* **393**, 801-805.

14. Anderson, K. S., Sikorski, J. A., and Johnson, K. A. (1988) *Biochemistry* 27, 7395-7406.
15. Marquardt, J. L., Brown, E. D., Walsh, C. T., and Anderson, K. S. (1993) *J. Am. Chem. Soc.* 115, 10398-10399.
16. Kim, D. H., Lees, W. J., Haley, T. M., and Walsh, C. T. (1995) *J. Am. Chem. Soc.* 117, 1494-1502.
17. Kim, D. H., Lees, W. J., and Walsh, C. T. (1994) *J. Am. Chem. Soc.* 116, 6478-6479.
18. Walker, M. C., and Jones, C. R. (1992) *J. Am. Chem. Soc.* 114, 7601-7603.
19. Skarzynski, T., Kim, D. H., Lees, W. J., Walsh, C. T., and Duncan, K. (1998) *Biochemistry* 37, 2572-2577.
20. Sack, S., Dauter, Z., Wanke, C., Amrhein, N., Mandelkow, E., and Schonbrunn, E. (1996) *J. Struct. Biol.* 117, 73-76.
21. Anderson, K. S., Sikorski, J. A., and Johnson, K. A. (1988) *Biochemistry* 27, 1604-1610.
22. Castellino, S., Leo, G. C., Sammons, D., and Sikorski, J. A. (1989) *Biochemistry* 28, 3856-3868.
23. Bondinell, W. E., Vnek, J., Knowles, P. F., Sprecher, M., and Sprinson, D. B. (1971) *J. Biol. Chem.* 246, 6191-6196.
24. Brown, E. D., Marquardt, J. L., Lee, J. P., Walsh, C. T., and Anderson, K. S. (1994) *Biochemistry* 33, 10638-10645.
25. Schonbrunn, E., Eschenburg, S., Luger, K., Kabsch, W., and Amrhein, N. (2000) *Proc. Natl. Acad. Sci. U. S. A.* 97, 6345-6349.
26. Schonbrunn, E., Eschenburg, S., Krekel, F., Luger, K., and Amrhein, N. (2000) *Biochemistry* 39, 2164-2173.
27. Anton, D. L. H., L.; Fish, S.M.; Abeles, R.H. (1983) *Biochemistry* 22, 5903-5908.
28. An, M. M., U.; Neidlen, U.; Bartlett, P.A. (2003) *J. Am. Chem. Soc.* 125, 12759-12767.
29. Krekel, F. S., A.K.; Macheroux, P.; Amrhein, N.;

- Evans, J.N. (2000) *Biochemistry* 39, 12671-12677.
30. Mized, S., Wright, J. E., Byczynski, B., and Berti, P. J. (2003) *Biochemistry* 42, 6986-6995.
 31. Samland, A. K., Etezady-Esfarjani, T., Amrhein, N., and Macheroux, P. (2001) *Biochemistry* 40, 1550-1559.
 32. Huynb, Q. K. K., G. M.; Bild, G.S. (1988) *J. Biol. Chem.* 263, 735-739.
 33. Eschenburg, S. K., W.; Healy, M.L.; Schonbrunn, E. (2003) *J. Biol. Chem.* 278, 49215-49222.
 34. Radzicka, A., and Wolfenden, R. (1995) *Science* 267, 90-93.
 35. Alexander, J. K. (1961) *J. Bacteriol.* 81, 903-910.
 36. Tsumuraya, Y., Brewer, C. F., and Hehre, E. J. (1990) *Arch. Biochem. Biophys.* 281, 58-65.
 37. Mieval, J. J., Simon, M., and Abeles, R. H. (1972) *J. Biol. Chem.* 247, 532-542.
 38. Voet, J. G., and Abeles, R. H. (1970) *J. Biol. Chem.* 245, 1020-1031.
 39. Silverstein, R., Voet, J., Reed, D., and Abeles, R. H. (1967) *J. Biol. Chem.* 242, 1338-1346.
 40. Metzger, B., Helmreich, E., and Glaser, L. (1967) *Proc. Natl. Acad. Sci. U. S. A.* 57, 994-1001.
 41. Gold, A. M., and Osber, M. P. (1972) *Arch. Biochem. Biophys.* 153, 784-787.
 42. Byczynski, B., Mized, S., and Berti, P. J. (2003) *J. Am. Chem. Soc.* 125, 12541-12550.
 43. Lagunas, R. (1980) *Arch. Biochem. Biophys.* 205, 67-75.
 44. Lagunas, R. (1970) *Biochim. Biophys. Acta* 220, 108-115.
 45. Jaffe, K., and Apitz-Castro, R. (1977) *FEBS Lett.* 80, 115-118.
 46. Chasteen, N. D. (1983) *Struct. Bond.* 53, 105-138.

47. Nour-Eldeen, A. F., Craig, M. M., and Gresser, M. J. (1985) *J. Biol. Chem.* **260**, 6836-6842.
48. Pannifer, A. D., Flint, A. J., Tonks, N. K., and Barford, D. (1998) *J. Biol. Chem.* **273**, 10454-10462.
49. Schlichting, I., and Reinstein, J. (1999) *Nat. Struct. Biol.* **6**, 721-723.
50. Wittinghofer, A. (1997) *Curr. Biol.* **7**, 682-685.
51. Becke, A. D. (1988) *Phys. Rev. A* **38**, 3098-3100.
52. Perdew, J. P., and Wang, Y. (1992) *Phys. Rev. B* **45**, 13244.
53. Frisch, M. J. T., G. W.; Schlegel, H. B.; Scuseria, G. E.; Robb, M. A.; Cheeseman, J. R.; Zakrzewski, V. G.; Montgomery, J. A.; Stratmann, R. E.; Burant, J. C.; Dapprich, S.; Millam, J. M.; Daniels, A. D.; Kudin, K. N.; Strain, M. C.; Farkas, O.; Tomasi, J.; Barone, V.; Cossi, M.; Cammi, R.; Mennucci, B.; Pomelli, C.; Adamo, C.; Clifford, S.; Ochterski, J.; Petersson, G. A.; Ayala, P. Y.; Cui, Q.; Morokuma, K.; Malick, D. K.; Rabuck, A. D.; Raghavachari, K.; Foresman, J. B.; Cioslowski, J.; Ortiz, J. V.; Stefanov, B. B.; Liu, G.; Liashenko, A.; Piskorz, P.; Komaromi, I.; Gomperts, R.; Martin, R. L.; Fox, D. J.; Keith, T.; Al-Laham, M. A.; Peng, C. Y.; Nanayakkara, A.; Gonzalez, C.; Challacombe, M.; Gill, P. M. W.; Johnson, B. G.; Chen, W.; Wong, M. W.; Andres, J. L.; Head-Gordon, M.; Replogle, E. S.; Pople, J. A. (1998) *Gaussian 98(Revision A.6)*, Gaussian, Inc.: Pittsburgh, PA,.
54. Reed, A. E., Curtiss, L. A., and Weinhold, F. (1988) *Chem. Rev.* **88**, 899-926.
55. Dobson, G. P., Hitchins, S., and Teague, W. E. (2002) *J. Biol. Chem.* **277**, 27176-27182.
56. Lecoq, K., Belloc, K., Desgrangers, C., Konrad, M., and Daignan-Fronier, B. (2001) *J. Bacteriol.* **2001**, 4910-4913.
57. Kresge, A. J., Leibovitch, M., and Sikorski, J. A. (1992) *J. Am. Chem. Soc.* **114**, 2618-2622.
58. Mizyed, S., Oddone, A., Byczynski, B., Hughes, D. W., and Berti, P. J. (2005) *Biochemistry* **44**, 4011-4017.
59. Okumura, A. S., A.; Saruta, A.; Miki, M. (1996) *Bull. Chem. Soc. Jpn.*

- 69, 3021-3030.
60. Okumura, A. Y., N.; Okazaki, N. (1973) *Bull. Chem. Soc. Jpn.* **46**, 3633.
 61. Okumura, A. W., M.; Sakaue, M.; Okazaki, N. (1979) *Bull. Chem. Soc. Jpn.* **52**, 2783.
 62. Damitio, J. S., G.; Meany, J.E.; Pocker, Y. (1992) *J. Am. Chem. Soc.* **114**, 3081-3087.
 63. Pocker, Y. M., J.E.; Nist, B.J.; Zadorojny, C. (1969) *J. Phys. Chem.* **78**, 2879-2885.
 64. Gruys, K. J. M., M. R.; Pansegrau, P. D.; Sikorski, J. A. (1993) *Biochem. Biophys.* **304**, 345-351.
 65. Kumler, W. D., and Eiler, J. J. (1943) *J. Am. Chem. Soc.* **65**, 2355-2361.
 66. Bailey, N., Carrington, A., Lott, K. A. K., and Symons, M. C. R. (1960) *J. Chem. Soc.*, 290-297.
 67. Bjerrum, J., Schwarzenbach, G., and Sillen, L. G. (1958) *Stability constants of metal-ion complexes, with solubility products of inorganic substances*, International Union of Pure and Applied Chemistry.
 68. Kline, P. C., and Schramm, V. L. (1993) *Biochemistry* **1993**, 13212-13219.
 69. Schoevaart, R. R., F.; Sheldon, R.A. (2001) *J. Org. Chem.* **66**, 4559-4562.
 70. Long, J. W., and Ray, W. J. (1973) *Biochemistry* **12**, 3932-3937.
 71. Lagunas, R. (1970) *Biochem. Biophys. Acta.* **220**, 108-115.
 72. M. E. Clark, personal communication
 73. O'Neal, C. C., Bild, G. S., and Smith, L. T. (1983) *Biochemistry* **83**, 611-618.
 74. Macheroux, P. (1998) *Biochem. J.* **335**, 319.

75. Dreyfuss, J. (1964) *J. Biol. Chem.* 239, 2292-2297.
76. O'Brien, P. J., and Herschlag, D. (2002) *Biochemistry* 41, 3207-3225.

